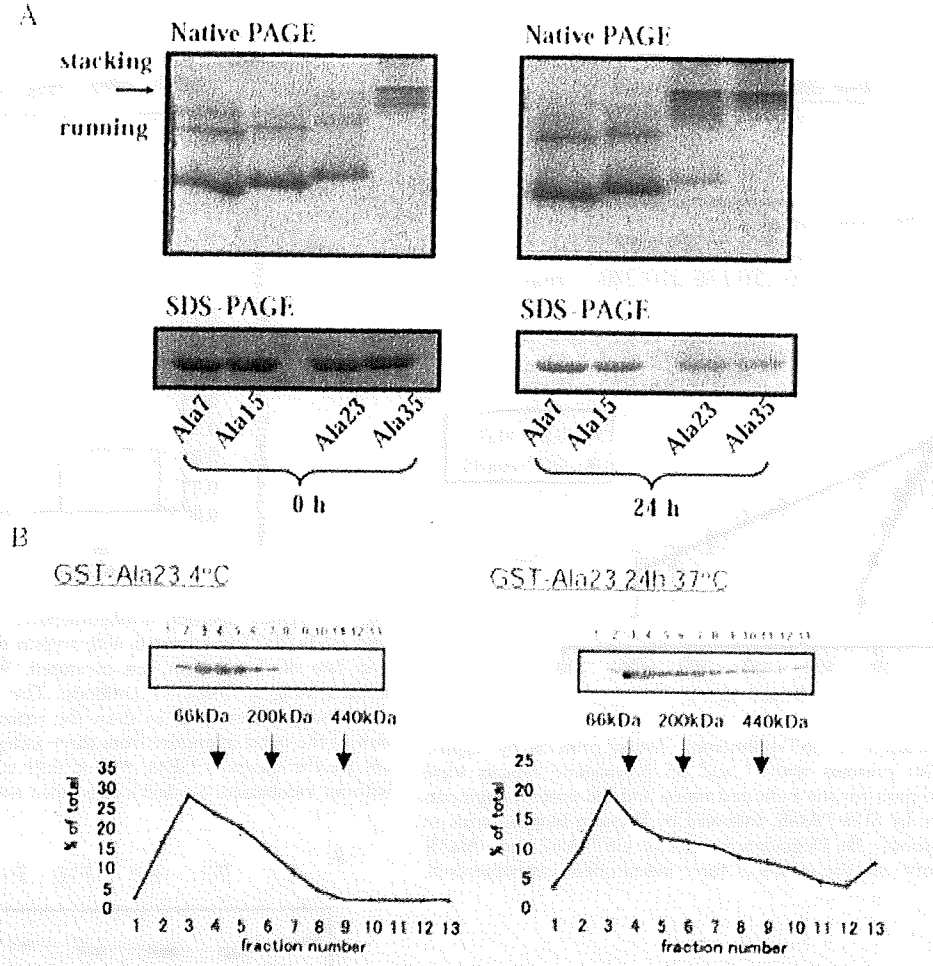


Fig. 3. Mobility shift of purified GST-Ala23 after long-term incubation. **A:** GST-Ala was incubated at 37°C for 24 hr and subjected to analysis by native- and SDS-PAGE. The proteins were stained with Coomassie brilliant blue. **B:** Fractionation of GST-Ala23 with or without long-term incubation by sucrose density gradient centrifugation. The amount of GST-Ala23 present in each fraction was assessed by Western blotting with an anti-GST antibody

lymeric proteins such as Hoxd13, Hoxa13, Runx2, and Sox3 that were expressed in COS-1 cells (Albrecht et al., 2004). Because movement of proteins from the cytoplasm to the nucleus may be precluded by their oligomerization status, we analyzed the oligomerization of proteins containing polyalanine repeat tracts.

Our results showed that YFP-Ala23 and YFP-Ala35 oligomerized within the cells and that these proteins were heterogeneous in form. At a length considered to be pathological in polyalanine diseases, i.e., ~20 polyalanine residues, the proteins were unstable and were prone to oligomerization. Indeed, monomer to oligomer formation was recently reported for GFP-polyQ proteins expressed in COS cells (Takahashi et al., 2007). Collectively, these data suggest that the onset of polyglutamine and polyalanine diseases may relate to the oligomerization status of the disease-causing protein and that oligomerization itself is facilitated by the homopolymeric sequences. We previously found that polyalanine tracts were associated with mitochondria (Toriumi et al., 2008). Chaperone proteins such as Hsp40 and Hsp70 were also colocalized with aggregates formed by mutant PABPN1 having polyalanine expansion (Wang et al., 2005). Therefore, interacting proteins may be important for polyalanine oligomerization.

Proteins such as tumor necrosis factor-α (TNF-α) have short polyalanine repeats that make the protein resistant to degradation (Sharipo et al., 2001). Our studies show that oligomerized GST-fusion proteins are resistant to trypsin digestion and that large complexes are more resistant to trypsin digestion than smaller proteins. Furthermore, oligomerization of the proteins having long

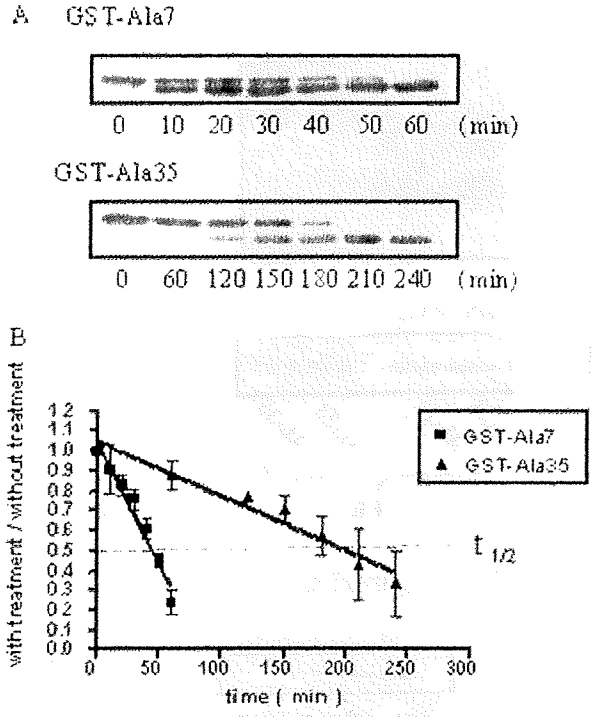


Fig. 4. Degradation of GST-polyalanine fusion proteins by trypsin. **A:** GST-fusion proteins with 7 and 35 polyalanine repeats were treated with trypsin for the indicated times, and the protein fragments were separated by SDS-PAGE, followed by Western blotting with an anti-GST antibody. **B:** Degradation rates of GST-Ala7 and -Ala35; the results shown are the means of three independent experiments ± SEM.

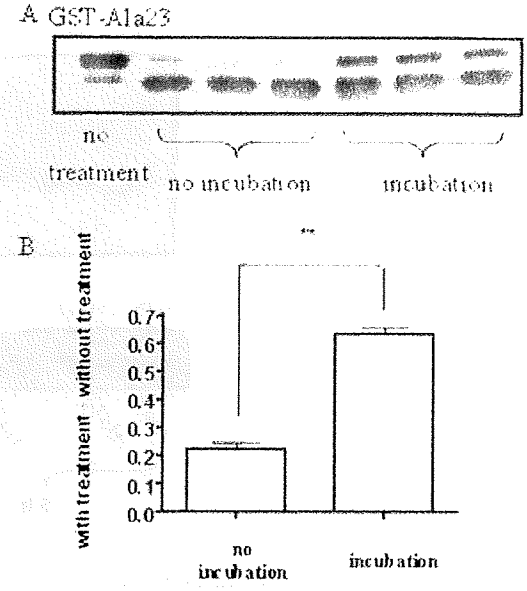


Fig. 5. Trypsin digestion of oligomerized GST-Ala23. **A:** Oligomerized GST-Ala23 was treated with trypsin for 1 hr, and the degradation rate of the protein was measured. Western blotting was performed using an anti-GST antibody. The assay was performed with three independent tubes to show the reproducibility. **B:** Quantification of the band intensities from three independent experiments. Values are the means ± SEM. $^{**}P < 0.01$ compared with GST-Ala23 without incubation. Student's two-tailed *t*-test.

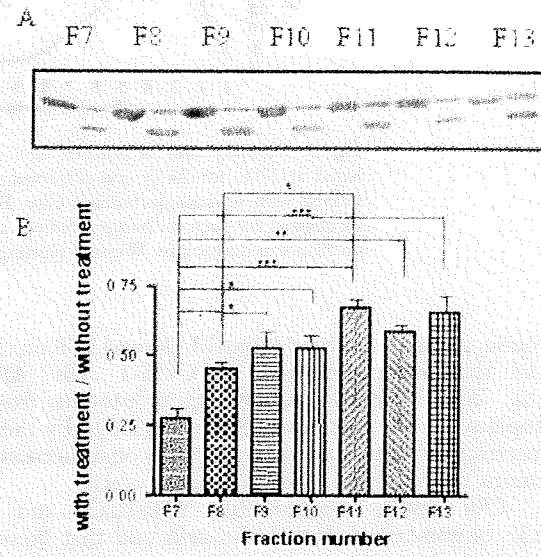


Fig. 6. Trypsin digestion of GST-Ala35. **A:** GST-Ala35 was left untreated (left) or treated (right) and separated by density gradient centrifugation. The proteins were then incubated with trypsin for 30 min, and Western blot analysis was performed with an anti-GST antibody. **B:** Quantification of the band intensities from three independent experiments. Values are means ± SEM. $^{*}P < 0.05$, $^{**}P < 0.01$, $^{***}P < 0.001$ compared with GST-Ala35 without treatment. ANOVA and post hoc Tukey's test were used as statistical tests.

polyalanine repeats prevented their translocation to the nucleus (Oma et al., 2007). Therefore, it is possible that oligomerized polyalanine repeat proteins in cytosol are toxic, because other fusion proteins that oligomerize as a result of excessive polyglutamine repeats, such as thioredoxin fusion protein, are toxic to cultured cells (Nagai et al., 2007).

After dialysis in the absence of reducing agents, GST-Ala23 oligomerized within 24 hr at 37°C. When reducing agents such as DTT were added to the solution, oligomerization did not occur. Therefore, reducing agents appear to inhibit oligomerization of homopolymeric proteins in vitro. We were unable to find other inhibitors. Candidate inhibitors that have been reported include Congo red (Heiser et al., 2000), polyglutamine binding peptide 1 (QBP1; Nagai et al., 2000), dimethylsulfoxide (DMSO), trimethylamine n-oxide (TMAO), and glycerol (Paul, 2007). Compounds that inhibit the common mechanisms that promote cellular toxicity resulting from homopolymeric repeats, e.g., oligomerization, are attractive therapeutic targets that warrant further study.

## REFERENCES


Abu-Baker A, Messaed C, Laganiere J, Gaspar C, Brais B, Rouleau GA. 2003. Involvement of the ubiquitin-proteasome pathway and molecular chaperones in oculopharyngeal muscular dystrophy. Hum Mol Genet 12:2609–2623.

Alba MM, Guigo R. 2004. Comparative analyis of amino acid repeats in rodents and humans. Genome Res 14:549–554.

Albrecht A, Mundlos S. 2005. The other trinucleotide repeat: polyalanine expansion disorders. Curr Opin Genet Dev 15:285–293.

Albrecht AN, Kornak U, Boddrich A, Suring K, Robinson PN, Stiege AC, Lurz R, Stricker S, Wanker EE, Mundlos S. 2004. A molecular pathogenesis for transcription factor associated poly-alanine tract expansions. Hum Mol Genet 13:2351–2359.

Becher MW, Kotzuk JA, Davis LE, Bear DG. 2000. Intranuclear inclusions in oculopharyngeal muscular dystrophy contain poly(A) binding protein 2. Ann Neurol 48:812–815.

Dehay B, Bertolotti A. 2006. Critical role of the proline-rich region in huntingtin for aggregation and cytotoxicity in yeast. J Biol Chem 281:35608–35615.

Giri K, Bhattacharyya NP, Basak S. 2007. pH-dependent self-assembly of polyalanine peptides. Biophys J 92:293–302.

Heiser V, Scherzinger E, Boeddrich A, Nordhoff E, Lurz R, Schugardt N, Lehrach H, Wanker EE. 2000. Inhibition of huntingtin fibrillogenesis by specific antibodies and small molecules: implications for Huntington's disease therapy. Proc Natl Acad Sci USA 97:6739–6744.

Nagai Y, Tucker T, Ren H, Kenan DJ, Henderson BS, Keene JD, Strittmatter WJ, Burke JR. 2000. Inhibition of polyglutamine protein aggregation and cell death by novel peptides identified by phage display screening. J Biol Chem 275:10437–10442.

Nagai Y, Inui T, Popiel HA, Fujikake N, Hasegawa K, Urade Y, Goto Y, Naiki H, Toda T. 2007. A toxic monomeric conformer of the polyglutamine protein. Nat Struct Mol Biol 14:332–340.

Oma Y, Kino Y, Sasagawa N, Ishiura S. 2004. Intracellular localization of homopolymeric amino acid-containing proteins expressed in mammalian cells. J Biol Chem 279:21217–21222.

Oma Y, Kino Y, Toriumi K, Sasagawa N, Ishiura S. 2007. Interactions between homopolymeric amino acids (HPAAs). Prot Sci 16:2195–2204.

Paul S. 2007. Polyglutamine-mediated neurodegeneration: use of chaperones as prevention strategy. Biochemistry 72:359–366.

Rankin J, Wyttenbach A, Rubinsztein DC. 2000. Intracellular green fluorescent protein-polyalanine aggregates are associated with cell death. Biochem J 348:15–19.

Shanmugam V, Dion P, Rochefort D, Laganiere J, Brais B, Rouleau GA. 2000. PABP2 polyalanine tract expansion causes intranuclear inclusions in oculopharyngeal muscular dystrophy. Ann Neurol 48:798–802.

Sharipo A, Imreh M, Leonchiks A, Brändén C, Masucci MG. 2001. cis-Inhibition of proteasomal degradation by viral repeats: impact of length and amino acid composition. FEBS Lett 499:137–142.

Shinchuk LM, Sharma D, Blondelle SE, Reixach N, Inouye H, Kirschner DA. 2005. Poly-(L-alanine) expansions form core beta-sheets that nucleate amyloid assembly. Proteins 61:579–589.

Takahashi Y, Okamoto Y, Popiel HA, Fujikake N, Toda T, Kinjo M, Nagai Y. 2007. Detection of polyglutamine protein oligomers in cells by fluorescence correlation spectroscopy. J Biol Chem 282:24039–24048.

Toriumi K, Oma Y, Kino Y, Futai E, Sasagawa N, Ishiura S. 2008. Expression of polyalanine stretches induces mitochondrial dysfunction. J Neurosci Res 86:1529–1537.

Wang Q, Mosser DD, Bag J. 2005. Induction of HSP70 expression and recruitment of HSC70 and HSP70 in the nucleus reduce aggregation of a polyalanine expansion mutant of PABPN1 in HeLa cells. Hum Mol Genet 14:3673–3684.

Neurochemistry International 54 (2009) 330–338

Contents lists available at ScienceDirect

Neurochemistry International

journal homepage: www.elsevier.com/locate/neuint

# Proteomic and histochemical analysis of proteins involved in the dying-back-type of axonal degeneration in the gracile axonal dystrophy (*gad*) mouse

Akiko Goto [a,b], Yu-Lai Wang [a], Tomohiro Kabuta [a], Rieko Setsuie [a], Hitoshi Osaka [a], Akira Sawa [c], Shoichi Ishiura [b], Keiji Wada [a,*]

[a] *Department of Degenerative Neurological Diseases, National Institute of Neuroscience, National Center of Neurology and Psychiatry, 4-1-1 Ogawahigashi, Kodaira, Tokyo, 187-8502, Japan*

[b] *Department of Life Sciences, Graduate School of Arts and Sciences, University of Tokyo, 3-8-1 Komaba, Meguro-ku, Tokyo,153-8902, Japan*

[c] *Depts. of Psychiatry and Neuroscience, Johns Hopkins University School of Medicine, Baltimore, MD 21287, USA*

ARTICLE INFO

*Article history:*
Received 24 November 2008
Received in revised form 12 December 2008
Accepted 17 December 2008
Available online 25 December 2008

*Keywords:*
Axonal degeneration
Dying-back
*gad* mouse
UCH-L1
Ubiquitin
2D-DIGE
GAPDH
Oxidative stress

ABSTRACT

Local axonal degeneration is a common pathological feature of peripheral neuropathies and neurodegenerative disorders of the central nervous system, including Alzheimer's disease, Parkinson's disease, and stroke; however, the underlying molecular mechanism is not known. Here, we analyzed the gracile axonal dystrophy (*gad*) mouse, which displays the dying-back-type of axonal degeneration in sensory neurons, to find the molecules involved in the mechanism of axonal degeneration. The *gad* mouse is analogous to a null mutant of ubiquitin carboxyl-terminal hydrolase L1 (UCH-L1). UCH-L1 is a deubiquitinating enzyme expressed at high levels in neurons, as well as testis and ovary. In addition, we recently discovered a new function of UCH-L1—namely to bind to and stabilize mono-ubiquitin in neurons, and found that the level of mono-ubiquitin was decreased in neurons, especially in axons of the sciatic nerve, in *gad* mice. The low level of ubiquitin suggests that the target proteins of the ubiquitin proteasome system are not sufficiently ubiquitinated and thus degraded in the *gad* mouse; therefore, these proteins may be the key molecules involved in axonal degeneration. To identify molecules involved in axonal degeneration in *gad* mice, we compared protein expression in sciatic nerves between *gad* and wild-type mice at 2 and 12 weeks old, using two-dimensional difference gel electrophoresis. As a result, we found age-dependent accumulation of several proteins, including glyceraldehyde-3-phosphate dehydrogenase (GAPDH) and 14-3-3, in *gad* mice compared with wild-type mice. Histochemical analyses demonstrated that GAPDH and 14-3-3 were localized throughout axons in both *gad* and wild-type mice, but GAPDH accumulated in the axons of *gad* mice. Recently, it has been suggested that a wide range of neurodegenerative diseases are characterized by the accumulation of intracellular and extracellular protein aggregates, and it has been reported that oxidative stress causes the aggregation of GAPDH. Furthermore, histochemical analysis demonstrated that sulfonated GAPDH, a sensor of oxidative stress that elicits cellular dysfunction, was expressed in the axons of *gad* mice, and 4-hydroxy-2-nonenal, a major marker of oxidative stress, was also only detected in *gad* mice. Our findings suggest that GAPDH may participate in a process of the dying-back-type of axonal degeneration in *gad* mice and may provide valuable insight into the mechanisms of axonal degeneration.



## 1. Introduction

Axonal degeneration occurs in several chronic neurodegenerative diseases and in injuries caused by, for example, toxic, ischemic, or traumatic insults. Recent findings suggest that axonal degeneration precedes, and sometimes causes, neuronal death in these neurodegenerative disorders (Li et al., 2001; Ferri et al., 2003; Fischer et al., 2004; Stokin et al., 2005; Fischer and Glass, 2007), but the underlying molecular mechanism is not known.

The gracile axonal dystrophy (*gad*) mutant mouse is characterized by sensory ataxia at an early stage, followed by motor ataxia at a later stage (Yamazaki et al. 1988; Saigoh et al., 1999). Pathologically, axonal degeneration in the *gad* mouse begins with the distal ends of primary ascending axons in the dorsal root ganglia (DRG) (Mukoyama et al., 1989; Kikuchi et al., 1990; Oda et al., 1992; Miura et al. 1993), and spheroid formation in the dying-back-type of axonal degeneration is observed in the gracile and dorsal spinocerebellar tracts (Yamazaki et al. 1988; Kikuchi

* Corresponding author. Tel.: +81 42 346 1715 fax: +81 42 346 1745.
*E-mail address:* wada@ncnp.go.jp (K. Wada).

0197-0186/$ – see front matter © 2008 Elsevier Ltd. All rights reserved.
doi:10.1016/j.neuint.2008.12.012

et al., 1990; Miura et al., 1993). At a later stage, axonal degeneration and spheroid formation are observed at both the central and peripheral ends of DRG neurons and extend transsynaptically to the upper tracts as well as to motor neurons (Mukoyama et al., 1989; Kikuchi et al., 1990; Oda et al., 1992; Miura et al., 1993). Therefore, the *gad* mouse is an effective model for analyzing the molecular mechanism of the dying-back-type of axonal degeneration.

Previously, we found that the *gad* mutation is caused by an in-frame deletion of *Uchl1*, which encodes ubiquitin carboxyl-terminal hydrolase L1 (UCH-L1) (Saigoh et al., 1999). UCH-L1 is expressed at high levels in neurons, as well as testis and ovary, and constitutes ~5% of total soluble protein in the brain (Wilkinson et al., 1989). UCH-L1 is reported to be one of the deubiquitinating enzymes in the ubiquitin-proteasome system (UPS), where it hydrolyzes bonds between ubiquitin (Ub) and small adducts and creates free mono-Ub *in vitro* (Larsen et al. 1998). UCH-L1 also acts as a Ub ligase *in vitro* (Liu et al., 2002). In addition, we recently found a new function for UCH-L1—to bind to and stabilize mono-Ub in neurons (Osaka et al., 2003).

Using histochemical analysis, we previously demonstrated that UCH-L1 and mono-Ub are colocalized in axons of the sciatic nerve. In *gad* mice, the level of mono-Ub was decreased in neurons, especially in axons of the sciatic nerve (Osaka et al., 2003). The low level of ubiquitin suggests that the target proteins of the ubiquitin-proteasome system (UPS) are not sufficiently ubiquitinated and thus degraded in the *gad* mouse; therefore, these proteins may be key molecules involved in axonal degeneration. To identify the molecules involved in axonal degeneration in *gad* mice, we analyzed protein expression in sciatic nerves using two-dimensional difference gel electrophoresis (2D-DIGE).

Proteomic approaches compare protein expression comprehensively; 2D-DIGE is a modification of the traditional 2D technology, in which small amounts of multiple protein samples can be compared together, because each sample can be pre-labeled with different fluorescence dyes, mixed together, and run on the same isoelectric focusing (IEF) gel and SDS-PAGE (Knowles et al., 2003; Shaw and Riederer, 2003). We used 2D-DIGE because it is the most efficient method for analyzing the small amount of protein that can be extracted from a sciatic nerve. Here, we show that there are age-dependent accumulations of several proteins, including glyceraldehyde-3-phosphate dehydrogenase (GAPDH) and 14-3-3, in *gad* mice compared with wild-type (WT) mice, suggesting that these proteins are involved in axonal degeneration.

## 2. Experimental procedures

### 2.1. Animals

We used homozygous *gad* mice and their wild-type siblings (Harada et al. 2004; Wang et al. 2004). Mice were maintained and propagated at the National Institute of Neuroscience, National Center of Neurology and Psychiatry, Japan. Proteomic studies were carried out at 2 and 12 weeks old. Western blotting analyses were carried out at 12 weeks old. Histochemical analyses were carried out at 7 and 12 weeks old. Animals were anesthetized with Nembutal, and the sciatic nerve was perfused with saline. All mouse experiments were performed in accordance with our institution's regulations for animal care and with the approval of the Animal Investigation Committee of the National Institute of Neuroscience, National Center of Neurology and Psychiatry which conforms to the National Institute of Health guide for the care and use of laboratory animals.

### 2.2. Preparation of protein samples and labeling of protein samples with Cy dyes

Each sciatic nerve was suspended in 300 μl of sample buffer, containing 7 M urea, 2 M thiourea, 4% (w/v) CHAPS, and 40 mM Tris base (pH 8.0), by sonication for 60 s on ice, gently vortexed, and centrifuged for 20 min at 14,000 × *g* at 4 °C. Protein concentration was determined using a 2-D Quant Kit (GE Healthcare, Piscataway, NJ, USA). Protein samples were labeled as recommended by the manufacturer (GE Healthcare) using 400 pmol Cy dyes (GE Healthcare) per 50 μg of protein. Separate solutions containing 15 μg of protein from one *gad* or WT sample were labeled with Cy3 or Cy5 dye, respectively, and a common pool of proteins with *gad* and WT samples mixed equally were labeled with Cy2 dye by vortexing and incubating on ice in the dark for 30 min. The labeled samples were quenched by the addition of 1 μl 10 mM lysine (Sigma–Aldrich, St. Louis, MO, USA) and incubated on ice for 10 min.

### 2.3. Two-dimensional polyacrylamide gel electrophoresis (2D PAGE)

The quenched Cy3, Cy5, and Cy2 samples (15 μg of protein each) were mixed and denatured in 2D PAGE sample buffer containing 7 M urea, 2 M thiourea, 4% (w/v) CHAPS, 0.2% DTT, and 1.4% Ampholine. For the IEF, 45 μg of protein was applied to a rehydrated Immobiline Drystrip (pH 3–10, 7 cm; GE Healthcare) in a strip holder and incubated overnight in the dark. IEF was performed using a Multiphor II Electrophoresis system (GE Healthcare). The electrophoresis conditions were set as follows: step 1, 200 V for 1 min; step 2, 3500 V for 90 min; step 3, 3500 V for 125 min. After IEF, the strip was equilibrated with SDS buffer and applied to the 12.5% 2D SDS-PAGE for the analysis of 12-week-old mice and to the 4–20% SDS-PAGE for the analysis of 2-week-old mice using a precast Multigel II system (Daiichi Kagaku, Japan).

### 2.4. Image analysis and statistics

We scanned 2D gels using a Typhoon 9000 fluorescent imager (GE Healthcare). Excitation/emission wavelengths were chosen for each of the dyes. Gel images were preprocessed to remove extraneous areas using ImageQuant V5.0 (GE Healthcare). Gel analysis was performed using DeCyder DIA V5.0 (Difference In-gel Analysis; GE Healthcare). In-gel matching and statistical analysis were performed using DeCyder BVA V5.0 (Biological Variance Analysis; GE Healthcare). The Student's paired *t*-test ($P < 0.05$) was performed to identify the protein spots that were differentially expressed between *gad* and WT mice.

### 2.5. In-gel digestion and analysis by matrix-assisted laser desorption/ionization tandem time-of-flight (MALDI-TOF/TOF) mass spectrometry

To identify a particular protein in a spot detected by 2D-DIGE analysis, sciatic nerve extract containing 100 μg of protein was subjected to 12.5% 2D SDS-PAGE and stained with Coomassie brilliant blue (Invitrogen). The spots of interest were excised from the gel, destained, dehydrated with acetonitrile for 10 min, and completely dried under a vacuum pump for 10 min. Each spot was placed in 20 μl of 5 mM $NH_4HCO_3$ containing 1 pmol of sequencing-grade trypsin (Promega, Madison, WI, USA) overnight at 37 °C. Aliquots of the trypsinized samples were analyzed by nanoliquid chromatography and automatically spotted with alpha-cyano-4-hydroxy-cinnamic acid solution on a stainless-steel target and air dried. All mass spectra were obtained with MALDI-TOF/TOF (AXIMA-CFR; Shimadzu, Japan). MALDI peptide spectra were calibrated using several peaks of self-digested trypsin and matrix ion as internal standards.

### 2.6. Protein identification

Protein identification was performed using database searches on the web with Mascot Wizard (Matrix Science Ltd., London, United Kingdom). Criteria for protein identification were as follows: mascot score higher than 80 and mass tolerance of 100 ppm. Calculated pI and molecular mass data were obtained by Mascot.

### 2.7. 2D Western blotting for identification of GAPDH

One protein spot that was increased in *gad* mice but could not be detected by MALDI-TOF/TOF analysis was speculated to be GAPDH from its isoelectric point, molecular weight and location of the 2D gel compared with the mouse brain proteome database, and was therefore subjected to 2D Western blotting using an anti-GAPDH antibody (1:200, Chemicon, MAB374). One-hundred μg of sciatic nerve proteins were separated by 12.5% 2D SDS-PAGE and transferred onto a PVDF membrane (Immobilon-P; Millipore, Bedford, MA, USA). The membrane was washed with MilliQ water for 1 h at room temperature. Western blotting was performed as described in the following section.

### 2.8. Western blotting

Using 4–20% gradient SDS-PAGE, 2 μg of total protein was separated and transferred onto a PVDF membrane (Immobilon-P; Millipore). The membrane was washed with MilliQ water, then blocked with 5% skim milk in 0.05% Tween 20 in TBS (TTBS) for 1 h at room temperature, and incubated with primary antibodies in TTBS overnight at 4 °C. Primary antibodies used in this study were anti-UCH-L1 polyclonal antibody (1:5000, UltraClone, RA95101), anti-GAPDH monoclonal antibody (1:200, Chemicon, MAB374), anti-14-3-3 polyclonal antibody (1:100, IBL, 18649), anti-neurofilament L monoclonal antibody (NF-L, 1:500, Chemicon, MAB1615), anti-neuronal class III β tubulin antibody (βTUBIII, 1:1000, Covance, TUJ1), and anti-actin monoclonal antibody (1:4000, Sigma, AC-15). After washing, the membranes were incubated for 1 h at room temperature with either anti-mouse or anti-rabbit IgG horseradish peroxidase (HRP) conjugated secondary antibodies (1:10,000, GE Healthcare). Protein signals were detected with SuperSignal West Femto Maximum Sensitivity Substrate (Pierce) and were visualized with the LAS-3000 imaging system (Fujifilm, Tokyo, Japan).

*2.9. Immunohistochemistry*

Mice were anesthetized and perfused with ice-cold 4% paraformaldehyde in phosphate-buffered saline (PBS, pH 7.4). Sciatic nerves were collected and postfixed in 4% paraformaldehyde overnight at 4 °C. The samples were embedded in paraffin and sectioned at 5 μm for immunohistochemistry. Serial sections were deparaffinized in xylene and graded ethanol, and washed in distilled water. Sections were blocked by incubation in 10% normal goat serum for 30 min at room temperature and incubated overnight at 4 °C with diluted primary antibodies. The following antibodies were used at the final dilutions indicated: anti-GAPDH polyclonal antibody (1:1000), anti-sulfonated GAPDH polyclonal antibody (1:500; these two antibodies were kindly provided by Dr. Sawa), anti-14-3-3 polyclonal antibody (1:100, IBL, 18649), anti-myelin basic protein monoclonal antibody (MBP, 1:200, QED Bioscience, 24201), anti-neurofilament M monoclonal antibody (NF-M, 1:200, Chemicon, MAB1621), anti-UCH-L1 polyclonal antibody (1:2000, UltraClone, RA95101), anti-UCH-L1 monoclonal antibody (1:200; Medac, Wedel, Germany), βTUBIII (1:300, COVANCE, TUJ1), and anti-4-hydroxy-2-nonenal monoclonal antibody (HNE, 25 μg/ml, JaICA, Shizuoka, Japan).

After incubating with primary antibodies, sections were washed 5 times with 0.1% Tween 20 in PBS (PBST) for 5 min at room temperature and then incubated for 90 min at room temperature with diluted secondary antibodies. The following antibodies were used at the final dilutions indicated: anti-mouse-Alexa594 IgG and anti-rabbit-Alexa588 IgG (1:400, Invitrogen) for immunofluorescence staining, or EnVision+ anti-rabbit HRP (Dako, Japan) for DAB staining. For DAB staining, bound antibody complexes were visualized using DAB (Dako, Japan) as a peroxidase substrate. Primary and secondary antibodies were diluted in Dako Antibody Diluent (Dako, Japan). After incubation with secondary antibodies, sections were washed 5 times with PBST for 5 min at room temperature and mounted with Antifade Kit (Molecular Probes). For analysis of 14-3-3 and HNE, sections were pretreated in a microwave oven for 10 min in citrate buffer solution (pH 6.0), cooled down, and washed 3 times for 5 min in PBS at room temperature. For the other immunostaining analyses, this pretreatment was not needed. For DAB staining, sections were treated with 3% $H_2O_2$ in methanol for 5 min to quench endogenous peroxidase activity before treatment with the primary antibodies.

## 3. Results

### *3.1. Analyses of differentially expressed proteins between gad and WT mice by 2D-DIGE*

To find proteins that are upregulated in *gad* mice compared with WT mice, we analyzed sciatic nerves from 3 *gad* and 3 WT mice at 2 weeks old as well as at 12 weeks old, using 2D-DIGE technology. The proteins from *gad* mice were pre-labeled with Cy5 (red), and the proteins from WT mice were pre-labeled with Cy3 (green), respectively. A common pool of proteins composed of an equal amount of protein from a single *gad* and WT mouse was pre-labeled with Cy2, and the same manipulation was performed in 3 independent experiments.

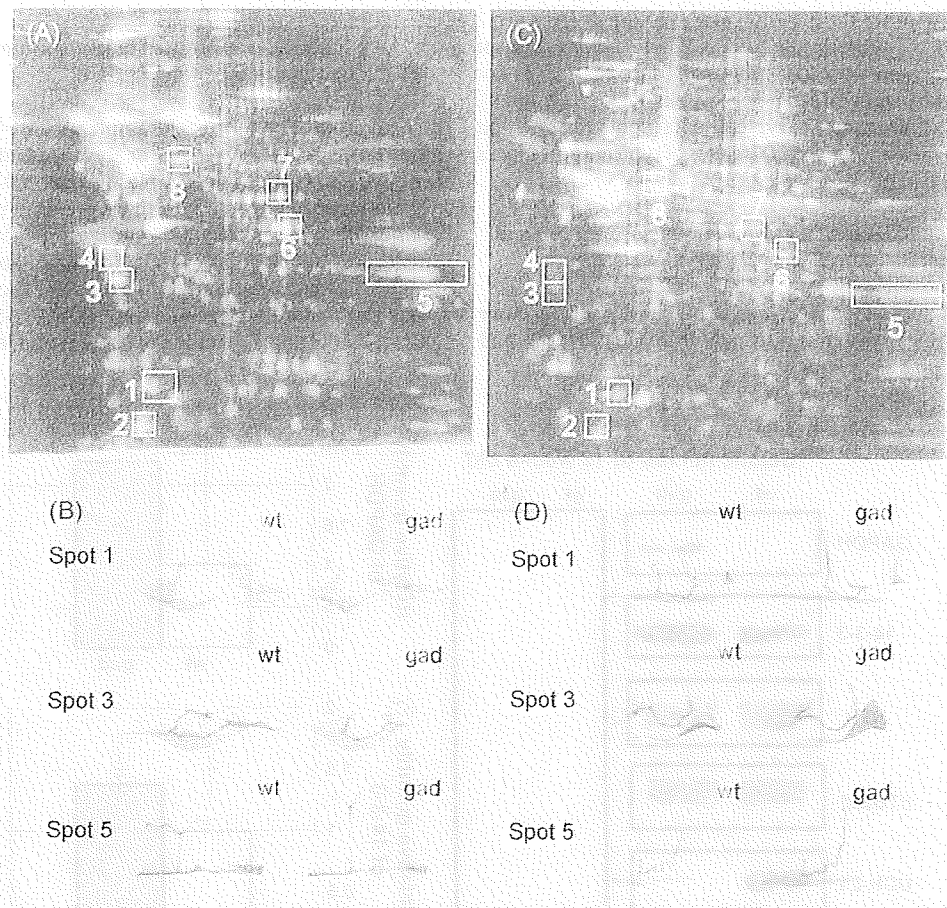


**Fig. 1.** Analyses of differentially expressed proteins between *gad* and wild-type mice by two-dimensional difference gel electrophoresis (2D-DIGE).
(A) A representative pseudocolor picture of superimposed DIGE images of mice at 12 weeks old. Fourteen protein spots are increased in *gad* mice compared with wild-type (WT) mice (red) by at least 1.6-fold (Student's paired *t*-test value; $P < 0.05$ in 3 parallel gels), and one spot is not detected at all in *gad* mice (green). Seven protein spots (spot No. 2–8) are increased in *gad* mice in an age-dependent manner, and one spot (spot No. 1) was not detected at all in *gad* mice at either 2 or 12 weeks old. The spot numbers of the latter differentiated 8 spots are shown in this map.
(B) A representative pseudocolor picture of superimposed DIGE images of mice at 2 weeks old. Eighteen protein spots are increased in *gad* mice compared with WT mice (red) by at least 1.6-fold (Student's paired *t*-test value; $P < 0.05$ in 3 parallel gels), and one spot is not detected at all in *gad* mice (green). The spot numbers in this figure are the same as in A.
(C) The 3D images of typical protein spots that were differentially expressed between *gad* and WT mice at 2 weeks old (spot numbers 1, 3, and 5 in A).
(D) The 3D images of typical protein spots that were differentially expressed between *gad* and WT mice at 2 weeks old (spot numbers 1, 3, and 5 in C) (For interpretation of the references to color in this figure legend, the reader is referred to the web version of the article.)

**Table 1**
List of proteins differentially expressed between *gad* and WT mice.

| Spot no. | Protein name | Score | Molecular mass (kDa)/pI | Av. ratio (*gad*/wt) 12 weeks | *P* value | Av. ratio (*gad*/wt) 2 weeks | *P* value |
|---|---|---|---|---|---|---|---|
| 1 | Ubiquitin thiolesterase PGP9.5 (UCH-L1) | 96 | 25.10/5.12 | −14.38 | 0.005 | −3.89 | 0.003 |
| 3 | 14-3-3 protein | 94 | 28.10/4.63 | 5.4 | 0.030 | 7.32 | 0.001 |
| 4 | Annexin A5 | 143 | 35.79/4.83 | 6.68 | 0.020 | 5.19 | 0.030 |
| 8 | Neurofilament triplet L protein (NF-L) | 212 | 61.40/4.62 | 2.18 | 0.010 | 3.53 | 0.026 |
| 5 | Glyceraldehyde 3-phosphate dehydrogenase (GAPDH) | | 38.07/8.34 | 3.89 | 0.043 | 1.61 | |

*GAPDH was detected by 2D Western blotting and not by MALDI-TOF/TOF.

Fig. 1A shows a representative pseudocolor picture of superimposed DIGE images of the 12-week-old mouse samples. Fourteen protein spots were increased by at least 1.6-fold in *gad* mice compared with WT mice (red; Student's paired *t*-test value; $P < 0.05$ in 3 parallel gels), and one spot was not detected at all in *gad* mice (green).

Fig. 1B shows a representative pseudocolor picture of superimposed DIGE images of the 2-week-old mouse samples. Eighteen protein spots were increased by at least 1.6-fold in *gad* mice compared with WT mice (red; Student's paired *t*-test value; $P < 0.05$ in 3 parallel gels), and one spot was not detected at all in *gad* mice (green).

Based on comparison of the 2D-DIGE analysis of mice between 2 and 12 weeks old, 7 protein spots showed an age-dependent increase in *gad* mice (spots No. 2–8). One spot (spot No. 1) was not detected at all in *gad* mice at either 2 or 12 weeks old (Fig. 1A and B).

Fig. 1C shows the 3D images of typical spots (spots No. 1, 3, and 5) in Fig. 1A, and Fig. 1D shows the 3D images of typical spots (spots No. 1, 3, and 5) in Fig. 1B.

### 3.2. Identification of differentially expressed proteins between gad and WT mice by MALDI-TOF/TOF and 2D Western blotting

The proteins of spots that were age dependently increased or absent in *gad* mice were analyzed by MALDI-TOF/TOF and identified (spots No. 1, 3, 4, and 8). The proteins were identified as UCH-L1 (spot No. 1), 14-3-3 (spot No. 3), annexin V (spot No. 4), and Neurofilament L (NF-L) (spot No. 8). Additionally, we speculated that spot No. 5 may represent GAPDH based on the information from the mouse brain proteome database (http://www.charite.de/humangenetik/klose_public1/index.html), and confirmed this by 2D Western blotting with GAPDH antibodies. The results of the protein identification are listed in Table 1, including spot number, protein name, mascot score, theoretical relative molecular mass, isoelectric point, average ratio of *gad*/wt protein level, and *P*-value using DeCyder, at both 2 and 12 weeks old.

### 3.3. Analyses of the expression levels of proteins in gad and WT mice by Western blotting

In 2D-DIGE system, each sample was pre-labeled with different fluorescence dyes, Cy3, Cy5 or Cy2. This labeling-process allows comparison of multiple samples in same 2D-gel, but it is reported that efficiency of each dyes to label proteins was not exactly the same. We assume that 2D-DIGE is reliable method to detect molecules involved in axonal degeneration but Western blot analysis using specific antibodies is more accurate, and in fact, it is usual that identified proteins by TOF-MASS are reconfirmed by Western blotting. Therefore, the expression levels of the proteins in

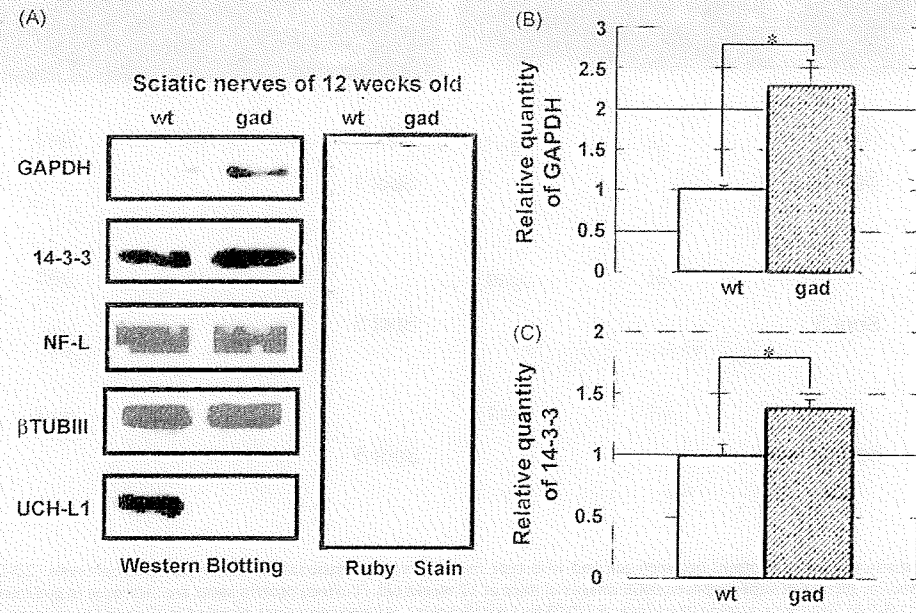


**Fig. 2.** Western blotting analyses of the expression levels of proteins expressed differentially between *gad* and WT mice.
(A) Results of Western blotting analysis with antibodies against ubiquitin carboxyl-terminal hydrolase L1 (UCH-L1), neurofilament L (NF-L), 14-3-3, glyceraldehyde-3-phosphate dehydrogenase (GAPDH), and classIII β tubulin (βTUBIII). GAPDH and 14-3-3 protein levels were increased in *gad* mice compared with WT mice.
(B) Quantification of the band intensities of GAPDH. Values are means ± SEM of 3 independent experiments (*$P < 0.05$); GAPDH is increased by about 2.3-fold in *gad* mice at 12 weeks old compared with WT mice.
(C) Quantification of the band intensities of 14-3-3. Values are means ± SEM of 3 independent experiments (*$P < 0.05$); 14-3-3 is increased by 1.3-fold in *gad* mice at 12 weeks old compared with WT mice.

*gad* and WT mice listed in Table 1 were further analyzed by Western blotting to reconfirm the results of 2D-DIGE (Fig. 2A). We chose these proteins because they were all reported to be expressed in neurons. In 12-week-old *gad* mice, GAPDH was increased by an average ratio of 2.3-fold (Fig. 2B), and 14-3-3 was increased by an average ratio of 1.3-fold (Fig. 2C) compared with WT mice. The levels of NF-L and βTUBIII, which was used as an internal control, showed no significant difference between *gad* and WT mice at 12 weeks old (Fig. 2A). Annexin V was not analyzed because its antibodies did not work in this experimental system containing urea and thiourea. The same results were obtained in 3 independent experiments.

### 3.4. Histochemical localization of GAPDH in the sciatic nerves of gad and WT mice

Sciatic nerves are composed internally of neuronal axons and externally of myelin derived from glial Schwann cells, and protein samples in the proteomic analysis were a mixture of axons and myelin. We examined the histological localization of GAPDH, which was dominantly increased in *gad* mice, by double immunofluorescence staining using an antibody against GAPDH and the neuronal markers neurofilament M (NF-M) or UCH-L1, or the Schwann cells marker myelin basic protein (MBP). In *gad* mice, GAPDH was colocalized with MBP (Fig. 3A, right panel) but was more dominantly colocalized with NF-M, a neuronal marker (Fig. 3A, left panel). These results suggest that GAPDH is mainly localized in axons in *gad* mice. In WT mice, GAPDH was colocalized with the neuronal marker UCH-L1 (Fig. 3B, left panel). Because UCH-L1 is the product of the gene defective in the *gad* mouse, UCH-L1 is not detected in *gad* mice (Fig. 3B, right panel). The same results were obtained in 3 independent experiments.

### 3.5. DAB staining analyses of GAPDH and 14-3-3 in the sciatic nerves of gad and WT mice

We examined in detail the localization of GAPDH in cross or vertical sections of sciatic nerve axons by DAB staining (Figs. 4A–F). In the cross-sections, GAPDH was localized in axons in both *gad* and WT mice and was remarkably accumulated in *gad* mice compared with WT mice (Fig. 4A and B). In vertical sections, GAPDH was also localized in axons in both *gad* and WT mice (Fig. 4C–F). Notably, aggregates of GAPDH were observed in *gad* mice but not in WT mice (Fig. 4E and F, arrow). Next, we examined the expression of 14-3-3, which was found to be increased in *gad* mice upon 2D-DIGE and Western blotting analyses. In both *gad* and WT mice, 14-3-3 was expressed in axons, and there was no significant difference between *gad* and WT mice (Fig. 4G–J). The same results were obtained in 3 independent experiments.

### 3.6. Histochemical analyses of sulfonated GAPDH in the sciatic nerves of gad and WT mice

It was reported that oxidative stress induces the oligomerization and aggregation of GAPDH (Cumming and Schubert, 2005 Nakajima et al., 2007), and in this study we found that GAPDH is accumulated in axons of *gad* mice that exhibit a dying-back-type of axonal degeneration. Thus, we postulated that oxidative stress would be increased in *gad* mice, and therefore examined the expression of sulfonated GAPDH (Hara et al., 2005), in the sciatic

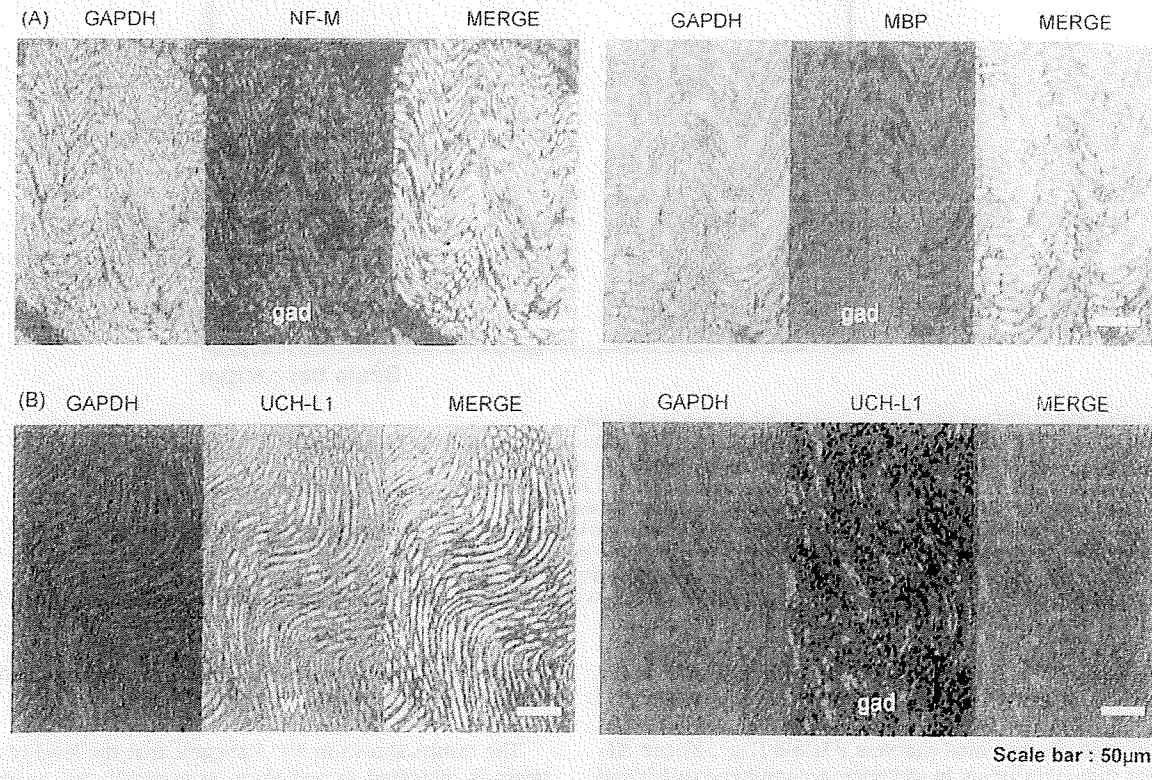


**Fig. 3.** Histochemical localization of GAPDH in the sciatic nerves of *gad* and WT mice.
(A) Double immunofluorescent staining of the sciatic nerve of *gad* mice using antibodies against GAPDH, neurofilament M (NF-M), or myelin basic protein (MBP). GAPDH was colocalized with NF-M (left panel) and partly with MBP (right panel) in *gad* mice. GAPDH is mainly localized in axons.
(B) Double immunofluorescent staining of the sciatic nerve of *gad* and WT mice using antibodies against GAPDH and UCH-L1. In WT mice, GAPDH is colocalized with UCH-L1 (left panel). In *gad* mice, UCH-L1 is not detected (right panel), and GAPDH is strongly detected compared with WT mice.

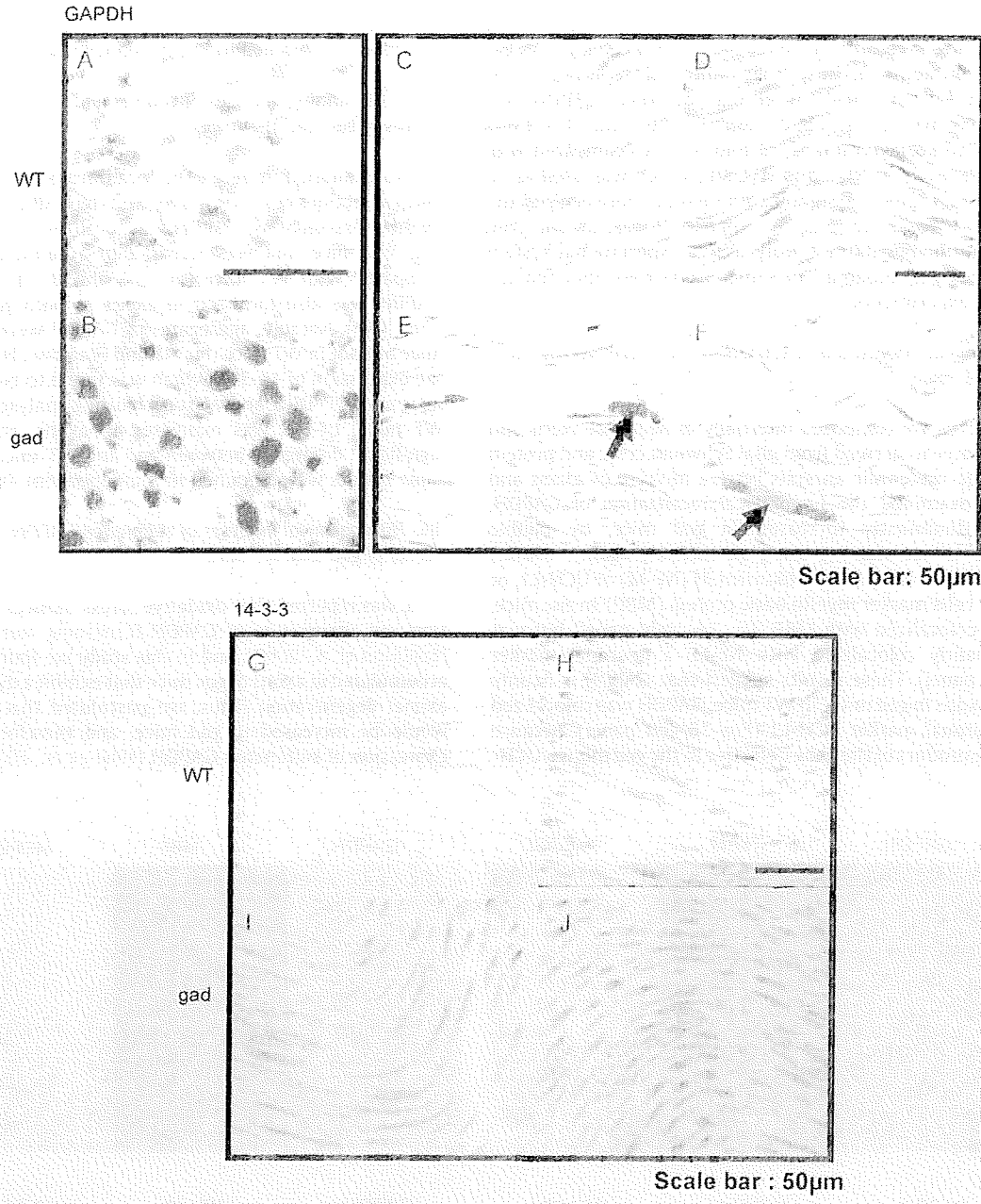


**Fig. 4.** DAB staining of GAPDH and 14-3-3 in the sciatic nerves of *gad* and WT mice.
(A–F) Sections of sciatic nerves of WT (A, C, and D) or *gad* (B, E, and F) mice stained with DAB using GAPDH antibodies.
(A) Cross-section of a sciatic nerve of a WT mouse. GAPDH is mainly localized in axons.
(B) Cross-section of a sciatic nerve of a *gad* mouse. GAPDH is mainly localized in axons and is highly expressed compared with the WT mouse.
(C and D) Vertical sections of sciatic nerves of WT mice. GAPDH is localized in axons.
(E and F) Vertical sections of sciatic nerves of *gad* mice. GAPDH is localized in axons and is accumulated. GAPDH aggregates are indicated by arrows.
(G–J) Sections of sciatic nerves of WT (G, H) and *gad* (I, J) mice stained with DAB using 14-3-3 antibodies.
(G and H) Vertical sections of sciatic nerves of WT mice; 14-3-3 is localized in axons of WT mice.
(I and J) Vertical sections of sciatic nerves of *gad* mice; 14-3-3 is localized in axons of *gad* mice, and there was no significant difference between *gad* and WT mice (G, H).

nerves of *gad* and WT mice. We found that although sulfonated GAPDH was not detected in WT mice, it was clearly detected in *gad* mice (Fig. 5A and B). In *gad* mice, sulfonated GAPDH was colocalized with the neuronal markers βTUBIII (Fig. 5B) and NF-M (data not shown) in axons. In *gad* mice, accumulated sulfonated GAPDH was also detected in the outer portion of the axons, around the DAPI staining for nuclei (Fig. 5C). Axons do not contain nuclei, so these DAPI signals may come from Schwann cells. The same results were obtained in 3 independent experiments.

### *3.7. Histological analyses of HNE, a marker of oxidative stress, in the sciatic nerves of gad and WT mice*

The results shown in Fig. 5 suggest that the level of oxidative stress is increased in *gad* mice. Accordingly, we examined the existence of HNE, a major marker of oxidative stress, in addition to sulfonated GAPDH. HNE was detected in *gad* mice, but not in WT mice (Fig. 6). The same results were obtained in 3 independent experiments.

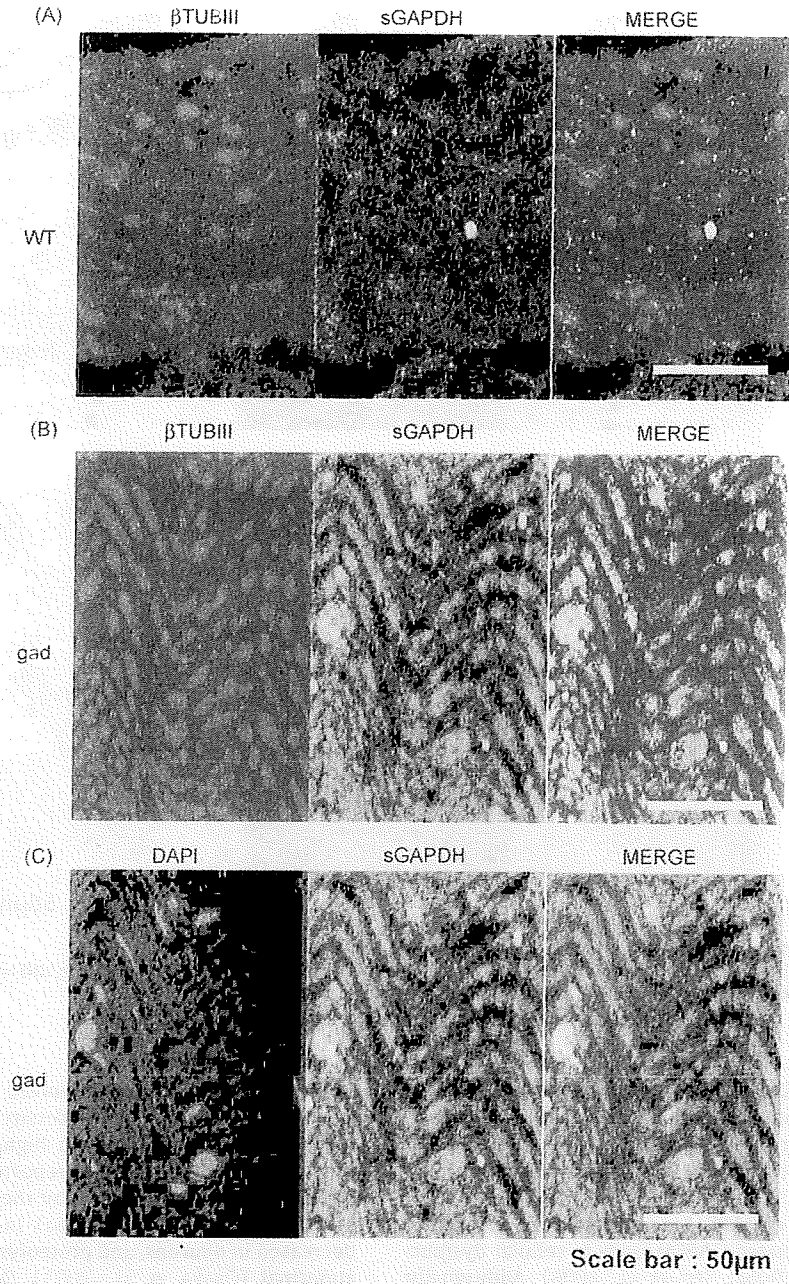


**Fig. 5.** Expression of sulfonated GAPDH in the sciatic nerves of *gad* and WT mice.
(A) Double immunofluorescent staining of a sciatic nerve of a WT mouse using antibodies against sulfonated GAPDH and βTUBIII. Sulfonated GAPDH was not detected in WT mice (middle panel).
(B) Double immunofluorescent staining of a sciatic nerve of a *gad* mouse using antibodies against sulfonated GAPDH and βTUBIII. In *gad* mice, sulfonated GAPDH was detected in axons of sciatic nerves (middle panel). Sulfonated GAPDH was colocalized with the neuronal marker βTUBIII in *gad* mice (right panel), as well as NF-M (data not shown). A representative result from 3 independent experiments is shown.
(C) Double immunofluorescent staining of a sciatic nerve of the *gad* mouse using an antibody against sulfonated GAPDH and DAPI. Sulfonated GAPDH was detected uniformaly within the axons of *gad* mice, and accumulation of sulfonated GAPDH was detected around the DAPI signals (right panel).

## 4. Discussion

In this study, we found that 14-3-3, annexin V, NF-L, and GAPDH were increased in an age-dependent manner in *gad* mice that display the dying-back-type of axonal degeneration, using 2D-DIGE analyses (Fig. 1). Based on Western blotting analyses, 14-3-3 and GAPDH were increased in *gad* mice compared with WT mice (Fig. 2). Histochemical analysis revealed that GAPDH was localized throughout axons and was accumulated in axons in *gad* mice compared with WT mice (Figs. 3 and 4). Also 14-3-3 was localized throughout axons, but there was no significant difference between *gad* and WT mice upon histochemical analyses, although it was increased in *gad* mice upon Western blotting analyses (Fig. 4). Since Western blotting showed only a slight increase in 14-3-3 (Fig. 2), we assume that this small difference could not be detected by histochemical analyses.

GAPDH is a classic glycolytic enzyme (Sirover 1999; Chuang et al. 2005), and recent studies show that it is multifunctional

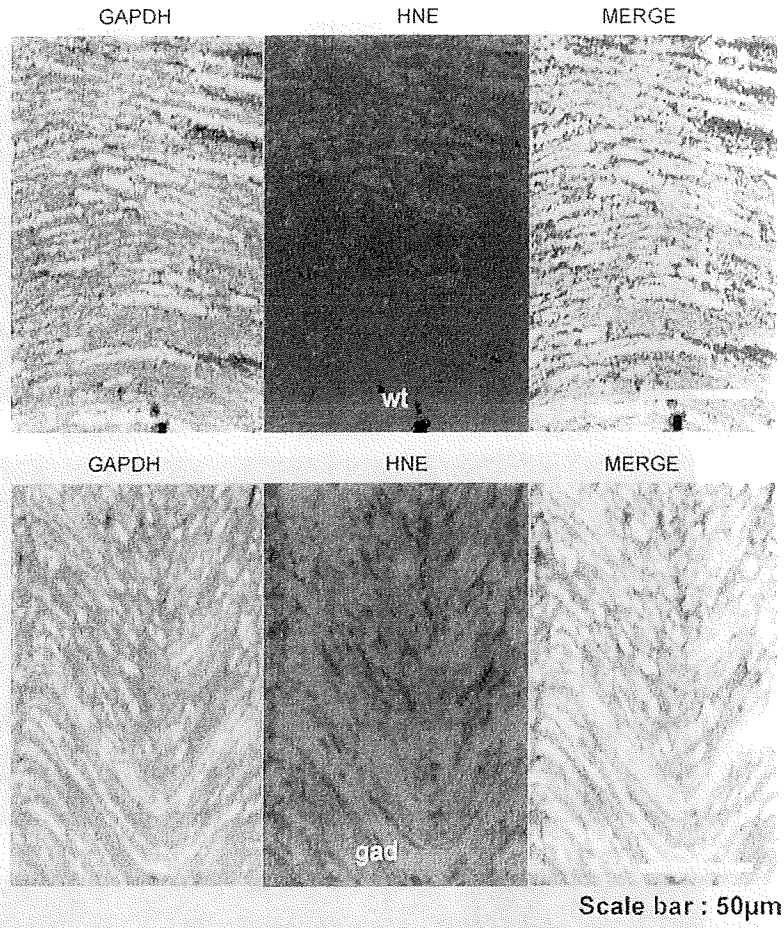


**Fig. 6.** Expression of HNE, a marker of oxidative stress, in the sciatic nerves of *gad* and WT mice.
Double immunofluorescent staining of sciatic nerves of *gad* and WT mice using antibodies against GAPDH and HNE. In WT mice, HNE was not detected (upper panel). On the other hand, HNE was strongly detected and mainly colocalized with GAPDH in *gad* mice (lower panel).

(Hara et al., 2006a). GAPDH has been reported to play roles in membrane fusion, microtubule bundling, nuclear RNA transport (Sirover 1999), and transcription (Zheng et al., 2003). Particularly, its role as a mediator for cellular dysfunction/death has been highlighted (Sawa et al., 1997; Ishitani et al., 1998; Hara et al., 2005, 2006b). Sulfonation of GAPDH is reported to be induced by oxidative stress, and sulfonated GAPDH leads to cellular dysfunction (Hara et al., 2005, 2006a; Sen et al., 2008). Additionally, oxidative stress induces the oligomerization and aggregation of GAPDH through aberrant disulfide bonding of active-site cysteines, which leads to the formation of insoluble aggregates *in vitro* (Cumming and Schubert, 2005; Nakajima et al., 2007). Thus, GAPDH appears to participate in the mechanism leading to cellular dysfunction/death induced by oxidative stress. However, its function in axons or its association with axonal degeneration has not yet been demonstrated.

In this study, we found that GAPDH and sulfonated GAPDH were accumulated in *gad* mice compared with WT mice, suggesting that oxidative stress is increased in *gad* mice. In fact, we found that the oxidative stress marker HNE is increased in *gad* mice. It has also been reported that, the levels of carbonyl modification of proteins that is caused by oxidative stress are increased in the brains of *gad* mice compared with WT mice (Castegna et al. 2004). Therefore, we assume that accumulation of GAPDH and sulfonated GAPDH in the axons of *gad* mice were induced by oxidative stress.

Various molecules are involved in reduction-oxidative reactions, and recently the necessity of the UPS in reduction-oxidative reactions has been highlighted (Okada et al., 1999; Kang et al., 2008). It has been reported that a number of oxidative stress sensors are regulated by the UPS (Iwai, 2003; Kobayashi et al., 2004, Hara et al. 2006a). In *gad* mice, free-Ub pools are decreased in neurons, and proteolysis in the UPS is thought to be abnormal (Osaka et al., 2003). Oxidative stress is therefore expected to be increased in *gad* mice, which is consistent with our findings.

There is another possible mechanism for the accumulation of GAPDH in the axons of *gad* mice. GAPDH is reported to be degraded mainly by chaperone-mediated autophagy (Aniento et al. 1993; Cuervo et al., 1997). Our recent study showed that UCH-L1 physically interacts with lysosome-associated membrane protein type 2A, which is a component of CMA (Kabuta et al. 2008); thus CMA is possibly altered in the neuronal system of *gad* mice, potentially leading to the accumulation of GAPDH in the axons of *gad* mice.

This study demonstrates the alteration of GAPDH in axons of the *gad* mouse, a mutant with a loss of function of UCH-L1. Our findings suggest that GAPDH may participate in the process leading to the dying-back-type of axonal degeneration in *gad* mice and may provide valuable insight into the mechanisms of axonal degeneration.

## Acknowledgements

We thank the following people for their contributions to this work: Dr. Hidemitsu Nakajima (Osaka Prefecture University), Dr. Satoshi Nagamine (National Center of Neurology and Psychiatry) and Dr. Makoto R. Hara (Johns Hopkins University School of Medicine) for helpful discussions; Ms. Hisae Kikuchi (National Center of Neurology and Psychiatry) for technical assistance with tissue sections; Ms. Masako Shikama (National Center of Neurology and Psychiatry) for the care and breeding of animals; Dr. Hayato Onishi (University of Tokyo) for assistance with the TOF MASS analysis; and Dr. H. Akiko Popiel (National Center of Neurology and Psychiatry) for support with English; Mitsubishi Tanabe Pharma Corporation for giving a chance to A.G. of admission to doctoral course. This work was supported in part by Grants-in-Aid for Scientific Research from the Ministry of Health, Labour and Welfare of Japan, Grants-in-Aid for Scientific Research from the Ministry of Education, Culture, Sports, Science and Technology of Japan, the Program for Promotion of Fundamental Studies in Health Sciences of the National Institute of Biomedical Innovation, and a grant from Japan Science and Technology Agency.

## References

Aniento, F., Roche, E., Cuervo, A.M., Knecht, E., 1993. Uptake and degradation of glyceraldehyde-3-phosphate dehydrogenase by rat liver lysosomes. J. Biol. Chem. 268, 10463–10470.

Castegna, A., Thongboonkerd, V., Klein, J., Lynn, B.C., Wang, Y.L., Osaka, H., Wada, K., Butterfield, D.A., 2004. Proteomic analysis of brain proteins in the gracile axonal dystrophy (gad) mouse, a syndrome that emanates from dysfunctional ubiquitin carboxyl-terminal hydrolase L-1, reveals oxidation of key proteins. J. Neurochem. 88, 1540–1546.

Chuang, D.M., Hough, C., Senatorov, V.V., 2005. Glyceraldehyde-3-phosphate dehydrogenase, apoptosis, and neurodegenerative diseases. Annu. Rev. Pharmacol. Toxicol. 45, 269–290.

Cuervo, A.M., Dice, J.F., Knecht, E., 1997. A population of rat liver lysosomes responsible for the selective uptake and degradation of cytosolic proteins. J. Biol. Chem. 272, 5606–5615.

Cumming, R.C., Schubert, D., 2005. Amyloid-beta induces disulfide bonding and aggregation of GAPDH in Alzheimer's disease. FASEB J. 19, 2060–2062.

Ferri, A., Sanes, J.R., Coleman, M.P., Cunningham, J.M., Kato, A.C., 2003. Inhibiting axon degeneration and synapse loss attenuates apoptosis and disease progression in a mouse model of motoneuron disease. Curr. Biol. 13, 669–673.

Fischer, L.R., Culver, D.G., Tennant, P., Davis, A.A., Wang, M., Castellano-Sanchez, A., Khan, J., Polak, M.A., Glass, J.D., 2004. Amyotrophic lateral sclerosis is a distal axonopathy: evidence in mice and man. Exp. Neurol. 185, 232–240.

Fischer, L.R., Glass, J.D., 2007. Axonal degeneration in motor neuron disease. Neurodegener. Dis. 4, 431–442.

Hara, M.R., Agrawal, N., Kim, S.F., Cascio, M.B., Fujimuro, M., Ozeki, Y., Takahashi, M., Cheah, J.H., Tankou, S.K., Hester, L.D., Ferris, C.D., Hayward, S.D., Snyder, S.H., Sawa, A., 2005. S-nitrosylated GAPDH initiates apoptotic cell death by nuclear translocation following Siah1 binding. Nat. Cell. Biol. 7, 665–674.

Hara, M.R., Cascio, M.B., Sawa, A., 2006a. GAPDH as a sensor of NO stress. Biochim. Biophys. Acta 1762, 502–509.

Hara, M.R., Thomas, B., Cascio, M.B., Bae, B.I., Hester, L.D., Dawson, V.L., Dawson, T.M., Sawa, A., Snyder, S.H., 2006b. Neuroprotection by pharmacologic blockade of the GAPDH death cascade. Proc. Natl. Acad. Sci. U.S.A. 103, 3887–3889.

Harada, T., Harada, C., Wang, Y.L., Osaka, H., Amanai, K., Tanaka, K., Takizawa, S., Setsuie, R., Sakurai, M., Sato, Y., Noda, M., Wada, K., 2004. Role of ubiquitin carboxy terminal hydrolase-L1 in neural cell apoptosis induced by ischemic retinal injury in vivo. Am. J. Pathol. 164, 59–64.

Ishitani, R., Tanaka, M., Sunaga, K., Katsube, N., Chuang, D.M., 1998. Nuclear localization of overexpressed glyceraldehyde-3-phosphate dehydrogenase in cultured cerebellar neurons undergoing apoptosis. Mol. Pharmacol. 53, 701–707.

Iwai, K., 2003. An ubiquitin ligase recognizing a protein oxidized by iron: implications for the turnover of oxidatively damaged proteins. J. Biochem. 134, 175–182.

Kabuta, T., Furuta, A., Aoki, S., Furuta, K., Wada, K., 2008. Aberrant interaction between Parkinson disease-associated mutant UCH-L1 and the lysosomal receptor for chaperone-mediated autophagy. J. Biol. Chem. 283, 23731–23738.

Kang, S.I., Choi, H.W., Kim, I.Y., 2008. Redox-mediated modification of PLZF by SUMO-1 and ubiquitin. Biochem. Biophys. Res. Commun. 369, 1209–1214.

Kikuchi, T., Mukoyama, M., Yamazaki, K., Moriya, H., 1990. Axonal degeneration of ascending sensory neurons in gracile axonal dystrophy mutant mouse. Acta Neuropathol. 80, 145–151.

Knowles, M.R., Cervino, S., Skynner, H.A., Hunt, S.P., de Felipe, C., Salim, K., Meneses-Lorente, G., McAllister, G., Guest, P.C., 2003. Multiplex proteomic analysis by two-dimensional differential in-gel electrophoresis. Proteomics 3, 1162–1171.

Kobayashi, A., Kang, M.I., Okawa, H., Ohtsuji, M., Zenke, Y., Chiba, T., Igarashi, K., Yamamoto, M., 2004. Oxidative stress sensor Keap1 functions as an adaptor for Cul3-based E3 ligase to regulate proteasomal degradation of Nrf2. Mol. Cell. Biol. 24, 7130–7139.

Larsen, C.N., Krantz, B.A., Wilkinson, K.D., 1998. Substrate specificity of deubiquitinating enzymes: ubiquitin C-terminal hydrolases. Biochemistry 37, 3358–3368.

Li, H., Li, S.H., Yu, Z.X., Shelbourne, P., Li, X.J., 2001. Huntingtin aggregate-associated axonal degeneration is an early pathological event in Huntington's disease mice. J. Neurosci. 21, 8473–8481.

Liu, Y., Fallon, L., Lashuel, H.A., Liu, Z., Lansbury Jr., P.T., 2002. The UCH-L1 gene encodes two opposing enzymatic activities that affect alpha-synuclein degradation and Parkinson's disease susceptibility. Cell 111, 209–218.

Miura, H., Oda, K., Endo, C., Yamazaki, K., Shibasaki, H., Kikuchi, T., 1993. Progressive degeneration of motor nerve terminals in GAD mutant mouse with hereditary sensory axonopathy. Neuropathol. Appl. Neurobiol. 19, 41–51.

Mukoyama, M., Yamazaki, K., Kikuchi, T., Tomita, T., 1989. Neuropathology of gracile axonal dystrophy (GAD) mouse. An animal model of central distal axonopathy in primary sensory neurons. Acta Neuropathol. 79, 294–299.

Nakajima, H., Amano, W., Fujita, A., Fukuhara, A., Azuma, Y.T., Hata, F., Inui, T., Takeuchi, T., 2007. The active site cysteine of the proapoptotic protein glyceraldehyde-3-phosphate dehydrogenase is essential in oxidative stress-induced aggregation and cell death. J. Biol. Chem. 282, 26562–26574.

Oda, K., Yamazaki, K., Miura, H., Shibasaki, H., Kikuchi, T., 1992. Dying back type axonal degeneration of sensory nerve terminals in muscle spindles of the gracile axonal dystrophy (GAD) mutant mouse. Neuropathol. Appl. Neurobiol. 18, 265–281.

Okada, K., Wangpoengtrakul, C., Osawa, T., Toyokuni, S., Tanaka, K., Uchida, K., 1999. 4-Hydroxy-2-nonenal-mediated impairment of intracellular proteolysis during oxidative stress. Identification of proteasomes as target molecules. J. Biol. Chem. 274, 23787–23793.

Osaka, H., Wang, Y.L., Takada, K., Takizawa, S., Setsuie, R., Li, H., Sato, Y., Nishikawa, K., Sun, Y.J., Sakurai, M., Harada, T., Hara, Y., Kimura, I., Chiba, S., Namikawa, K., Kiyama, H., Noda, M., Aoki, S., Wada, K., 2003. Ubiquitin carboxy-terminal hydrolase L1 binds to and stabilizes monoubiquitin in neuron. Hum. Mol. Genet. 12, 1945–1958.

Saigoh, K., Wang, Y.L., Suh, J.G., Yamanishi, T., Sakai, Y., Kiyosawa, H., Harada, T., Ichihara, N., Wakana, S., Kikuchi, T., Wada, K., 1999. Intragenic deletion in the gene encoding ubiquitin carboxy-terminal hydrolase in gad mice. Nat. Genet. 23, 47–51.

Sawa, A., Khan, A.A., Hester, L.D., Snyder, S.H., 1997. Glyceraldehyde-3-phosphate dehydrogenase: nuclear translocation participates in neuronal and nonneuronal cell death. Proc. Natl. Acad. Sci. U.S.A. 94, 11669–11674.

Sen, N., Hara, M.R., Kornberg, M.D., Cascio, M.B., Bae, B.I., Shahani, N., Thomas, B., Dawson, T.M., Dawson, V.L., Snyder, S.H., Sawa, A., 2008. Nitric oxide-induced nuclear GAPDH activates p300/CBP and mediates apoptosis. Nat. Cell. Biol. 10, 866–873.

Shaw, M.M., Riederer, B.M., 2003. Sample preparation for two-dimensional gel electrophoresis. Proteomics 3, 1408–1417.

Sirover, M.A., 1999. New insights into an old protein: the functional diversity of mammalian glyceraldehyde-3-phosphate dehydrogenase. Biochim. Biophys. Acta 1432, 159–184.

Stokin, G.B., Lillo, C., Falzone, T.L., Brusch, R.G., Rockenstein, E., Mount, S.L., Raman, R., Davies, P., Masliah, E., Williams, D.S., Goldstein, L.S., 2005. Axonopathy and transport deficits early in the pathogenesis of Alzheimer's disease. Science 307, 1282–1288.

Wang, Y.L., Takeda, A., Osaka, H., Hara, Y., Furuta, A., Setsuie, R., Sun, Y.J., Kwon, J., Sato, Y., Sakurai, M., Noda, M., Yoshikawa, Y., Wada, K., 2004. Accumulation of beta- and gamma-synucleins in the ubiquitin carboxyl-terminal hydrolase L1-deficient gad mouse. Brain Res. 1019, 1–9.

Wilkinson, K.D., Lee, K.M., Deshpande, S., Duerksen-Hughes, P., Boss, J.M., Pohl, J., 1989. The neuron-specific protein PGP 9.5 is a ubiquitin carboxyl-terminal hydrolase. Science 246, 670–673.

Yamazaki, K., Wakasugi, N., Tomita, T., Kikuchi, T., Mukoyama, M., Ando, K., 1988. Gracile axonal dystrophy (GAD), a new neurological mutant in the mouse. Proc. Soc. Exp. Biol. Med. 187, 209–215.

Zheng, L., Roeder, R.G., Luo, Y., 2003. S phase activation of the histone H2B promoter by OCA-S, a coactivator complex that contains GAPDH as a key component. Cell 114, 255–266.

ELSEVIER

Brain & Development 31 (2009) 465–468

BRAIN & DEVELOPMENT
Official Journal of the Japanese Society of Child Neurology

www.elsevier.com/locate/braindev

Case report

# A novel *POMT2* mutation causes mild congenital muscular dystrophy with normal brain MRI

Terumi Murakami [a,b], Yukiko K. Hayashi [a,*], Megumu Ogawa [a], Satoru Noguchi [a], Kevin P. Campbell [c], Masami Togawa [d], Takehiko Inoue [d], Akira Oka [d], Kousaku Ohno [d], Ikuya Nonaka [a], Ichizo Nishino [a]

[a] *Department of Neuromuscular Research, National Institute of Neuroscience, National Center of Neurology and Psychiatry, 4-1-1 Ogawa-Higashi, Kodaira, Tokyo 187-8502, Japan*
[b] *Department of Pediatrics, Tokyo Women's Medical University, Tokyo, Japan*
[c] *Howard Hughes Medical Institute, Department of Molecular Physiology and Biophysics, Internal Medicine, and Neurology, University of Iowa Carver, College of Medicine, Iowa City, IA, USA*
[d] *Department of Child Neurology, Institute of Neurological Sciences, Tottori University Faculty of Medicine, Tottori, Japan*

Received 12 June 2008; received in revised form 18 July 2008; accepted 6 August 2008

**Abstract**

We report a patient harboring a novel homozygous mutation of c.604T > G (p.F202V) in *POMT2*. He showed delayed psychomotor development but acquired the ability to walk at the age of 3 years and 10 months. His brain MRI was normal. No ocular abnormalities were seen. Biopsied skeletal muscle revealed markedly decreased but still detectable glycosylated forms of alpha-dystroglycan (α-DG). Our results indicate that mutations in *POMT2* can cause a wide spectrum of clinical phenotypes as observed in other genes associated with α-dystroglycanopathy. Presence of small amounts of partly glycosylated α-DG may have a role in reducing the clinical symptoms of α-dystroglycanopathy.


*Keywords:* POMT2; α-Dystroglycan; α-Dystroglycanopathy; Congenital muscular dystrophy; Limb girdle muscular dystrophy; Brain MRI

## 1. Introduction

Alpha-dystroglycan (α-DG) is a surface membrane protein that links extracellular basal lamina and intracellular cytoskeleton. α-DG is a highly glycosylated protein mainly composed of unique *O*-mannosyl glycans. Reduced/altered glycosylation of α-DG causes a wide variety of muscular dystrophies including Walker–Warburg syndrome (WWS), muscle-eye-brain disease (MEB), Fukuyama-type congenital muscular dystrophy (FCMD), congenital muscular dystrophies type 1C and type 1D, and limb girdle muscular dystrophies (LGMD) type 2I, 2K to 2N. They are collectively called alpha-dystroglycanopathies (α-DGP). So far, six causative genes for α-DGP have been identified including *protein-O-mannosyl transferase 1* and *2* (*POMT1 and POMT2*), *protein O-mannose β-1,2-N-acetylglucosaminyltransferase* (*POMGnT1*), *fukutin* (*FKTN*), *fukutin-related protein* (*FKRP*), and *acetylglucosaminyl transferase-like protein* (*LARGE*). Here we report a mild congenital muscular dystrophy patient associated with a novel homozygous mutation in *POMT2*.

## 2. Case report

A 4-year-old Japanese boy, the only child from healthy consanguineous parents, was delivered uneventfully at full term. During few days after birth, he was

* Corresponding author. Tel.: +81 42 341 2711; fax: +81 42 346 1742.
*E-mail address:* hayasi_y@ncnp.go.jp (Y.K. Hayashi).

0387-7604/$ - see front matter © 2008 Elsevier B.V. All rights reserved.
doi:10.1016/j.braindev.2008.08.005

low spirited and showed sucking weakness. Floppiness was not prominent but serum CK levels were markedly elevated up to 33,000 IU/l (normal < 70). His condition was improved within 2 weeks, but serum CK levels were persistently higher than 1000 IU/l. His motor milestones were delayed and he could control his head at 5 months of age. At 6-month-old, he could not sit without support, and muscle weakness and atrophy were noticed in lower limbs. Deep tendon reflexes were normal. No high arched palate or macroglossia were seen. Enjoji Scale of Infant Analytical Development (ESID) at his age of 7 months revealed mild delay in body movement (developmental age was 4 months, expression of language: 5 months), and his DQ was 83. Brain computed tomography (CT) revealed no definite abnormalities. Nerve conduction study was normal. His motor functions developed gradually and he was able to walk without support at 3 years and 10 months old. Gowers' sign was positive. Mild calf hypertrophy was seen with no joint contractures (Fig. 1A). Deep tendon reflexes were normal except for diminished Achilles tendon reflexes. ESID performed at his age of 3 years and 11 months showed general developmental delay (body movement: 15 months, hand movement: 24 months, activity of daily living: 27 months, personal relations: 24 months, expression of language: 18 months, and comprehension of language: 24 months), and his DQ was 47. Brain magnetic resonance imaging at 4 years and 1-month-old revealed no notable anomaly or cortical dysplasia (Fig. 1B). Detailed ophthalmological examinations revealed no abnormalities. No cardiac involvement was detected by chest X-ray, electrocardiogram, and echocardiography.

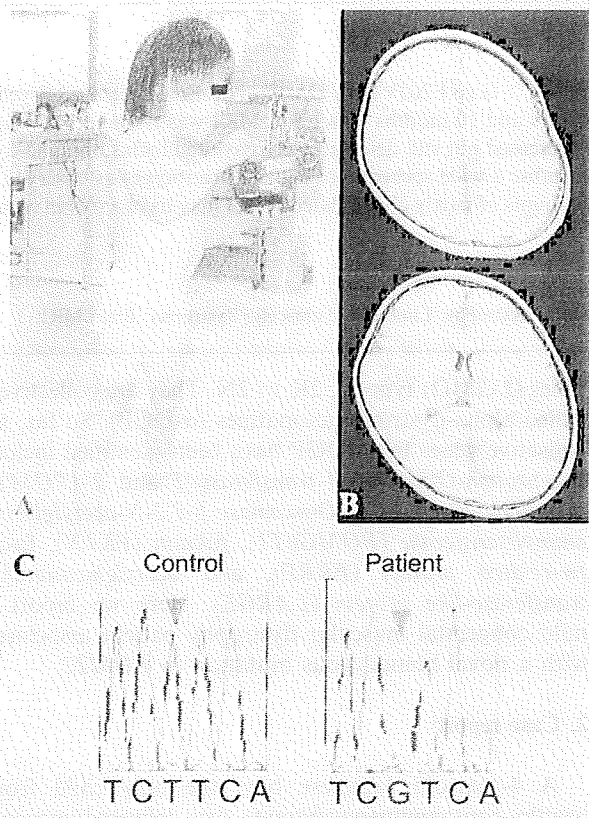


Fig. 1. (A) The patient can stand and walk with no support. Minimal calf hypertrophy is seen. (B) T2 weighted brain magnetic resonance imaging shows no obvious brain anomaly, cortical dysplasia, or white matter changes. (C) Sequence analysis of *POMT2* revealed a homozygous mutation at c.604T > G in exon 5.

Muscle biopsy taken at 7 months of age with informed consent showed dystrophic changes with scattered necrotic and regenerating fibers and mild endomysial fibrosis (Fig. 2A). No inflammatory changes were seen. On immunohistochemistry, glycosylated forms of α-DG detected by VIA4-1 antibody (Upstate Biotechnology, NY) was markedly reduced in the sarcolemma, while immunoreactions for the core region of α-DG using GT20ADG antibody [1] (data not shown) and for β-DG (43DAG1/8D5; Novocastra Laboratories, UK) was well preserved (Fig. 2A). On immunoblotting analysis, faint, broad band of around 140 kDa in size was detected by VIA4-1, whereas GT20ADG recognized a band of around 90 kDa in size. Laminin overlay assay showed barely detectable binding product (Fig. 2B). These results suggested altered glycosylation of α-DG in the muscle.

We performed mutation screening in all six causative genes for α-DGP. Genomic DNA was extracted from peripheral lymphocytes using standard technique after informed consent. Primer sequences we used are available on request. All exons and their franking intronic regions were directly sequenced by ABI PRISM 3100 (PE Applied Biosystems, CA). We identified a homozygous missense mutation of c.604T > G (p.F202V) in exon 5 of *POMT2* (Fig. 1C), which is not described in previous publications [3–8] and the mutation database (http://www.dmd.nl/).

The protein *O*-mannosyltransferase (POMT) activity was measured as previously described [2]. Mutant POMT2 (F202V) co-expressed with POMT1 in COS cells showed barely detectable POMT activity (data not shown).

## 3. Discussion

*POMT2* is the gene encoding an enzyme for protein *O*-mannosylation, and it is required to form a complex with POMT1 for the enzyme activity [2]. Recently, some patients with mutations in *POMT2* have been reported [3–8]. Most patients showed floppiness at birth, delayed psychomotor development, congenital muscular dystrophy, and severe mental retardation with or without ocular involvement. Brain anomalies are prominent including hydrocephalus, lissencephaly, agenesis of the corpus callosum, fusion of the hemispheres, and cerebel-

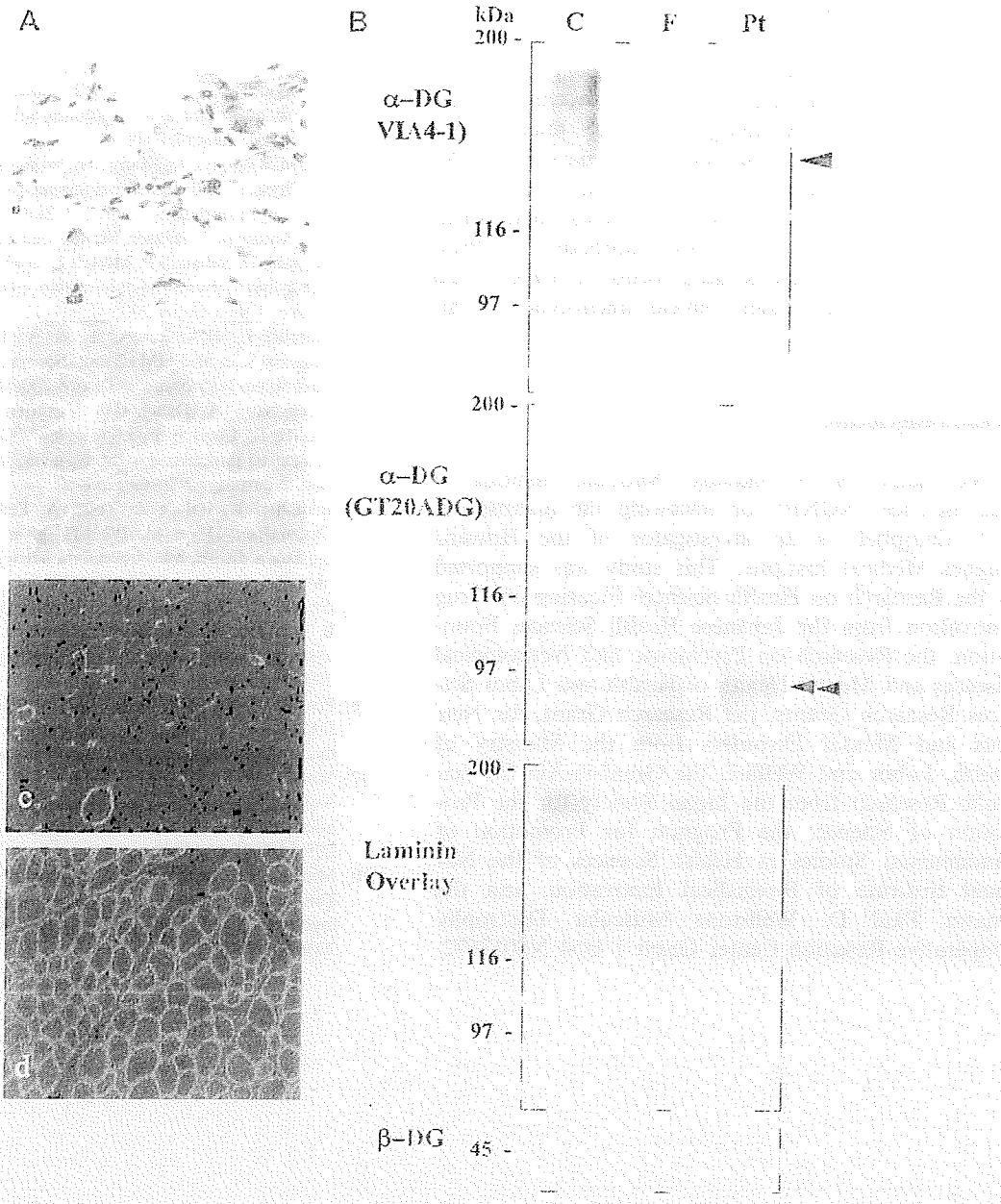


Fig. 2. (A) Histological analysis. On Hematoxylin and eosin (a) and modified Gomori-trichrime (b) staining, variation in fiber size and scattered necrotic and regenerating fibers are seen. Immunohistochemical analysis using antibodies VIA4-1 (c), which recognize heavily glycosylated form of α-dystroglycan (α-DG), showed greatly reduced sarcolemmal staining in patient, but well preserved immunoreactivities of β-DG (d) is seen. Bar = 50 m. (B) Immunoblotting analysis. Immunoblotting analysis using antibodies of VIA4-1, GT20ADG for α-dystroglycan (α-DG) and laminin overlay assay are performed using skeletal muscle from control (C), Fukuyama-type congenital muscular dystrophy (FCMD; F), and the patient (Pt). VIA4-1 recognizes a broad band about 156 kDa in size in control, and approximately 90 kDa in FCMD. In the patient muscle, reduced in size and amount compared with control was observed. GT20ADG revealed bands at approximately 90 kDa in both the patient and FCMD muscles. Laminin overlay assay shows barely detectable band in both the patient and FCMD.

lar hypoplasia [3–5]. In contrast, the patient reported here shows milder clinical features. Although his psychomotor milestones were delayed, he achieved independent ambulation with no marked brain malformation and ocular involvement. His clinical phenotype was intermediate between congenital muscular dystrophy and limb girdle muscular dystrophy. Milder clinical features with mutations in *POMT2* have been recently reported and designated as limb girdle muscular dystrophy type 2N [6,7]. Mutations in *POMT2* can cause wide spectrum of clinical phenotypes from Walker–Warburg syndrome to limb girdle muscular dystrophy (LGMD),

as demonstrated in patients with *FKRP*, *FKTN*, or *POMT1* mutations.

Pathological changes of skeletal muscle also showed mild dystrophic changes consistent with clinical findings. Clinical and pathological severity may not be always correlated to the molecular mass of α-DG [9]. However, some clinically milder patients with α-DGP show reduced but positive glycosylated forms of α-DG detected by the VIA4-1 antibody [10]. Preservation of partly glycosylated forms of α-DG could contribute to the milder clinical phenotype of this patient.

## Acknowledgements

We thank Dr. S. Shalaby (National Institute of Neuroscience, NCNP) for reviewing the manuscript. K.P. Campbell is an investigator of the Howard Hughes Medical Institute. This study was supported by the Research on Health Sciences focusing on Drug Innovation from the Japanese Health Sciences Foundation, the Research on Psychiatric and Neurological Diseases and Mental Health of Health and Labor Sciences Research Grants, the Research Grant, for Nervous and Mental Disorders from the Ministry of Health, Labor and Welfare, the Grant-in-Aid for Scientific Research from the Japan Society for the Promotion of Science, the Program for Promotion of Fundamental Studies in Health Sciences of the National Institute of Biomedical Innovation, and the Senator Paul D. Wellstone Muscular Dystrophy Cooperative Research Center Grant 1 U54 NS053672.

## References

[1] Kim DS, Hayashi YK, Matsumoto H, Ogawa M, Noguchi S, Murakami N, et al. POMT1 mutation results in defective glycosylation and loss of laminin-binding activity in alpha-DG. Neurology 2004;62:1009–11.

[2] Akasaka-Manya K, Manya H, Nakajima A, Kawakita M, Endo T. Physical and functional association of human protein *O*-mannosyltransferases 1 and 2. J Biol Chem 2006;281:19339–45.

[3] van Reeuwijk J, Janssen M, van den Elzen C, Beltran-Valero de Bernabe D, Sabatelli P, Merlini L, et al. POMT2 mutations cause alpha-dystroglycan hypoglycosylation and Walker–Warburg syndrome. J Med Genet 2005;42:907–12.

[4] Mercuri E, D'Amico A, Tessa A, Berardinelli A, Pane M, Messina S, et al. POMT2 mutation in a patient with 'MEB-like' phenotype. Neuromuscul Disord 2006;16:446–8.

[5] Yanagisawa A, Bouchet C, Van den Bergh PY, Cuisset JM, Viollet L, Leturcq F, et al. New POMT2 mutations causing congenital muscular dystrophy: identification of a founder mutation. Neurology 2007;69:1254–60.

[6] Biancheri R, Falace A, Tessa A, Pedemonte M, Scapolan S, Cassandrini D, et al. POMT2 gene mutation in limb-girdle muscular dystrophy with inflammatory changes. Biochem Biophys Res Commun 2007;363:1033–7.

[7] Godfrey C, Clement E, Mein R, Brockington M, Smith J, Talim B, et al. Refining genotype phenotype correlations in muscular dystrophies with defective glycosylation of dystroglycan. Brain 2007;130:2725–35.

[8] Peat RA, Smith JM, Compton AG, Baker NL, Pace RA, Burkin DJ, et al. The diagnosis and etiology of congenital muscular dystrophy. Neurology 2007 [Epub ahead of print].

[9] Matsumoto H, Hayashi YK, Kim DS, Ogawa M, Murakami T, Noguchi S, et al. Congenital muscular dystrophy with glycosylation defects of alpha-dystroglycan in Japan. Neuromuscul Disord 2005;15:342–8.

[10] Murakami T, Hayashi YK, Noguchi S, Ogawa M, Nonaka I, Tanabe Y, et al. Fukutin gene mutations cause dilated cardiomyopathy with minimal muscle weakness. Ann Neurol 2006;60:597–602.

J Neuropathol Exp Neurol

Vol. 68, No. 6
June 2009
pp. 701–707

ORIGINAL ARTICLE

# Defective Myotilin Homodimerization Caused by a Novel Mutation in *MYOT* Exon 9 in the First Japanese Limb Girdle Muscular Dystrophy 1A Patient

Sherine Shalaby, MD, Hiroaki Mitsuhashi, PhD, Chie Matsuda, PhD, Narihiro Minami, MS, Satoru Noguchi, PhD, Ikuya Nonaka, MD, PhD, Ichizo Nishino, MD, PhD, and Yukiko K. Hayashi, MD, PhD

**Abstract**

Myotilin is a muscle-specific Z disk protein. Several missense mutations in the myotilin gene (*MYOT*) have been identified in limb girdle muscular dystrophy (LGMD), myofibrillar myopathy, and distal myopathy patients. All previously reported pathogenic *MYOT* mutations have been identified only in Exon 2. We sequenced *MYOT* in 138 patients diagnosed as having LGMD, myofibrillar myopathy, or distal myopathy, and identified a novel *MYOT* mutation in Exon 9 encoding the second immunoglobulin-like domain in 1 patient with clinically typical LGMD. By light microscopy, there were scattered fibers with rimmed vacuoles and myofibrillary disorganization in the patient's muscle biopsy; accumulation of Z disk proteins was observed by immunohistochemistry. Immunoblot analysis demonstrated that the amount of myotilin monomer was increased in the patient muscle, but that the myotilin homodimeric band was decreased. Functional analysis of the myotilin mutation using a yeast 2-hybrid system revealed defective homodimerization of the mutant myotilin and decreased interaction between mutant myotilin and α-actinin. The homodimerization defect was further demonstrated by immunoprecipitation. This is the first *MYOT* mutation outside of Exon 2 in an LGMD type 1A patient and the first *MYOT* mutation identified in the Japanese population. This mutation in the second immunoglobulin-like domain impairs myotilin dimerization and alters the binding between myotilin and α-actinin, which is known to be important for actin bundling.

**Key Words**: Distal myopathy, Homodimer, Immunoglobulin-like domain, Limb girdle muscular dystrophy, Myofibrillar myopathy, Myotilin, Myotilinopathy.

## INTRODUCTION

Myotilin (myofibrillar protein with titin-like immunoglobulin domains) is a sarcomeric Z disk protein encoded by the myotilin gene (*MYOT* or *TTID*) on chromosome 5q31 (1). Myotilin is composed of a unique serine-rich N-terminus and 2 immunoglobulin-like domains at the C-terminus (1–4). Myotilin forms a homodimer and interacts with α-actinin (1), actin (5), and filamin C (FLNC) (6, 7) at the Z disk through these immunoglobulin-like domains (Fig. 1A). Myotilin is highly expressed in skeletal muscle, cardiac muscle, and peripheral nerves (1). Myotilin plays a significant role in sarcomere assembly by acting together with α-actinin and FLNC to cross-link actin filaments into tightly packed bundles (1, 5, 8). The resulting structures support the integrity of the contracting muscle cell (6).

Missense mutations in *MYOT* cause myofibrillar myopathy (MFM) (9–11), limb girdle muscular dystrophy type 1A (LGMD1A) (11–13) and late-onset distal myopathy (14, 15). These myotilinopathies are usually associated with cardiac involvement and peripheral neuropathy and rarely with respiratory involvement. Currently, there are only 8 known *MYOT* mutations associated with myopathy (i.e. K36E, S39F, S55F, T57I, S60C, S60F, Q74K, and S95I) (8–11); all are located in Exon 2 encoding the serine-rich amino-terminal (Fig. 1A).

Here, we report the first Japanese LGMD1A patient associated with a novel mutation in the second immunoglobulin-like domain of myotilin and provide data suggesting the pathobiologic significance of this mutation.

## MATERIALS AND METHODS

### Clinical Materials

All clinical materials used in this study were obtained for diagnostic purposes with informed consent. We searched

From the Department of Neuromuscular Research, National Institute of Neuroscience, National Center of Neurology and Psychiatry, Kodaira, Tokyo (SS, HM, SN, IN, IN, YKH); Neuroscience Research Institute, AIST, Central 6, Tsukuba, Ibaraki (CM); and Department of Laboratory Medicine, National Center Hospital of Neurology and Psychiatry, National Center of Neurology and Psychiatry, Kodaira, Tokyo (NM), Japan.

Send correspondence and reprint requests to: Yukiko K. Hayashi, MD, PhD, Department of Neuromuscular Research, National Institute of Neuroscience, National Center of Neurology and Psychiatry, 4-1-1 Ogawahigashi-cho, Kodaira, Tokyo 187-8502, Japan; E-mail: hayasi_y@ncnp.go.jp

This study was supported by a grant-in-aid for scientific research and a grant-in-aid for exploratory research from the Japan Society for the Promotion of Science; by the Research on Psychiatric and Neurological Diseases and Mental Health of the Health Labour Sciences Research Grant and research grants (20B-12, 20B-13, 19A-4, and 19A-7) for Nervous and Mental Disorders from the Ministry of Health, Labour, and Welfare; by the Research on Health Sciences focusing on Drug Innovation from the Japanese Health Sciences Foundation; and by the Program for Promotion of Fundamental Studies in Health Sciences of the National Institute of Biomedical Innovation.

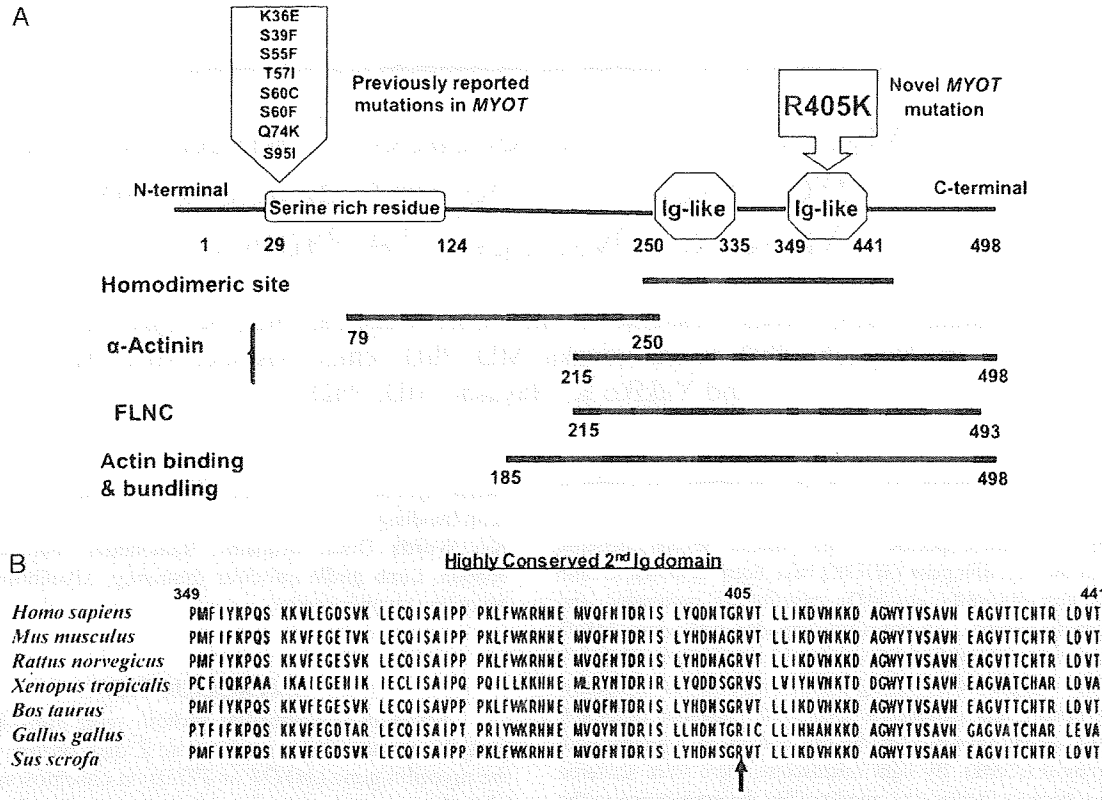


**FIGURE 1.** Myotilin structure, interacting partners, and reported mutations. **(A)** All previously reported mutations are located in the serine-rich domain; the novel mutation p.R405K identified in this study is located in the second immunoglobulin (Ig)-like domain of myotilin. Immunoglobulin domains of myotilin are regions of most myotilin interactions with other proteins. **(B)** The second Ig domain is highly conserved through species including the mutated residue p.R405 in the patient (arrow) (6–8). FLNC, filamin C.

for *MYOT* mutations in a total of 138 Japanese patients who had been diagnosed pathologically or clinically as MFM (n = 48), LGMD (n = 40), or distal myopathy (n = 50).

## Genetic Analysis

Genomic DNA was isolated from peripheral lymphocytes or muscle specimens using standard techniques. Nine sets of primers were used to amplify genomic fragments of *MYOT*. All exons and their flanking intronic regions of *MYOT* were sequenced directly in all 138 patients using an ABI PRISM 3100 automated sequencer (PE Applied Biosystems, Foster City, CA). Nearly all of the patients with the different diagnoses were screened for *ZASP*, *DES*, and *CRYAB* mutations. Distal myopathy patients were also screened for *GNE* mutations. Primer sequences are available on request.

## Histochemical Analysis

Biopsied muscle specimens were frozen in isopentane cooled in liquid nitrogen. Serial 10-μm cryosections were stained with hematoxylin and eosin, modified Gomori trichrome, nicotinamide adenine dinucleotide dehydrogenase-tetrazolium reductase, myosin ATPase phosphatase, and a battery of histochemical methods.

## Immunohistochemistry and Immunoblotting

Immunohistochemistry and immunoblotting were performed as previously described (13, 16, 17). Antibodies used in this study are to: myotilin (kindly provided by Dr Carpén, University of Helsinki) (13), desmin (Abcam, Tokyo, Japan), Z-band alternatively spliced PDZ motif protein (ZASP) (Abcam), skeletal muscle actin (Nichirei, Tokyo, Japan), and αB-crystallin (Stressgen, Victoria, British Columbia, Canada).

Antibodies to dystrophin (Novocastra Laboratories, Newcastle upon Tyne, UK), sarcoglycans (Novocastra), α-dystroglycan (Upstate Biotechnology, Lake Placid, NY), dysferlin (Novocastra), caveolin-3 (BD Transduction Laboratories, Lexington, KY), calpain-3 (Novocastra), merosin (Chemicon International, Temecula, CA), collagen VI (ICN Biomedicals, Inc, Cleveland, OH), and emerin (Novocastra) were also used in the LGMD patients to exclude other diagnosable causes of muscular dystrophy.

## Plasmid Construction

Total RNA was extracted from control human skeletal muscle using standard techniques; cDNA was synthesized by reverse transcription polymerase chain reaction with random hexamers. Full-length myotilin (wtMYOT), skeletal muscle

actin (ACTA1), α-actinin 2 (ACTN2), and the C-terminal portion (i.e. amino acids from 1967 to 2699) of FLNC were amplified using the following primers: MYOT, 5′-GGAATT CAGTAATAATTTGCCTTCA TCTTCCA-3′ and 5′-CGGGATCCACAAATCCATATACCCAGATTTCCT-3′; ACTA1, 5′-GGAATTCCAGAAACTAGACACAATGTG CGA-3′ and 5′-CGGGATCCAGTTGTTACAAAGAAAGT GACTGCG-3′; ACTN2, 5′-CCGGAATTCGCGGCCAC CATGGATTACAAGGATGACGACGACGATAAGAAC CAGATAGAGCCCGGCGT-3′ and 5′-CCGCTCGAGTCA CAGATCGCTCTCCCCGTA-3′; and FLNC, 5′-GGAATT CAAGATCACCGAGAGTGATCTGAGC-3′ and 5′-GTCGACCTCCTTGACAGTGTAGGTGACATTG-3′. The polymerase chain reaction products were cloned into the pGEM-T-easy vector (Promega, Madison, WI), and their sequences were confirmed. For expression in yeast, the cDNAs inserted in pGEM-T-easy were digested and ligated into the vectors pGBKT7 containing *GAL4* DNA-binding domain and pGADT7 containing *GAL4* activating domain (Takara Bio, Shiga, Japan). Mutant myotilin (mMYOT) (c.1214G>A) was generated by site-directed mutagenesis using the primers 5′-GATAACACTGGAAAAGTTACTTTACTG-3′ and 5′-CAGTAAAGTAACTTTTCCAGTGTTATC-3′.

## Yeast 2-Hybrid Experiment

Yeast 2-hybrid (Y2H) assays aimed at testing specific interaction pairs were carried out as previously described (18–20). *Saccharomyces cerevisiae AH109* was double transformed with pGBKT7 constructs and pGADT7 constructs and selected on minimal medium lacking leucine and tryptophan and containing histidine (SD/-Leu/-Trp/+His) plates (low-stringency plate). The transformants were picked up and spotted onto selective medium lacking histidine (SD/-Leu/-Trp/-His) plates with 0.2, 0.5, 1.0, 2.0, or 5.0 mmol/L 3-amino-1,2,4-triazole (3-AT), a competitive inhibitor of the HIS3 reporter gene (high-stringency plate) and plates without 3-AT (medium-stringency plate). The plates were then incubated at 30°C for 4 days, and the growth of the transformants was analyzed.

## Immunoprecipitation and Immunoblot Analysis

For expression in mammalian cells, wtMYOT or mMYOT inserted in pGADT7 were digested by *Eco*RI and *Bam*HI, and ligated into FLAG-tag-inserted pcDNA3.1/V5-HisA (kindly gifted by Dr Ishiura, University of Tokyo). The cDNAs inserted in pGADT7 were also digested by *Sfi*I and *Xho*I and ligated into pCMV-Myc vector (Takara Bio).

COS-7 cells were cultured in Dulbecco modified Eagle medium (Sigma, St Louis, MO) supplemented with 10% fetal bovine serum (Invitrogen, Carlsbad, CA) at 37°C in a humidified atmosphere of 5% carbon dioxide. The cells were transiently transfected using FuGENE HD transfection reagent (Roche Diagnostics, Indianapolis, IN) according to the manufacturer's instructions. Mouse horseradish peroxidase–conjugated anti-Myc antibody (9E10) was purchased from Santa Cruz Biotechnology (Santa Cruz, CA). Rabbit anti-FLAG polyclonal antibody was purchased from Sigma.

COS-7 cells were cotransfected with 5 μg of each plasmid. Forty-eight hours after transfection, the cells were then lysed in 1.0 mL of lysis buffer containing 20 mmol/L Tris-HCl (pH 7.5), 150 mmol/L NaCl, 10 mmol/L EDTA (pH 8.0), 10% glycerol, 1% Nonidet P-40, and Complete Protease Inhibitor Cocktail (Roche Diagnostics). The lysates were incubated at 4°C for 30 minutes with gentle rotation and then centrifuged at 15,000 × *g* at 4°C for 30 minutes. The supernatants were collected, and their protein concentrations were determined using the protein assay kit (Bio-Rad, Hercules, CA).

For immunoprecipitation, the protein concentration of the cleared lysates was adjusted to 1.5 μg/μL, and anti-FLAG M2 affinity gel (Sigma) was added. The mixtures were incubated at 4°C overnight. The resulting immune complexes were washed once with lysis buffer and 3 times with Tris buffered saline. The proteins were eluted by boiling at 95°C for 5 minutes in the sample buffer without reducing agent (50 mmol/L Tris-HCl [pH 6.8], 2% sodium dodecyl sulfate, 1% glycerol [vol/vol], 0.1% bromophenol blue), and resolved by sodium dodecyl sulfate–polyacrylamide gel electrophoresis. The polyacrylamide gel electrophoresis–separated proteins were transferred to Immobilon-P membranes (Millipore, Bedford, MA), and the membranes were blocked with blocking buffer (5% nonfat dry milk in PBS containing 0.05% Tween-20) at room temperature for 1 hour. The blocked membranes were incubated with a primary antibody at room temperature for 1 hour. Anti-Myc-horseradish peroxidase antibody was diluted in Can Get Signal solution 2 (Toyobo, Osaka, Japan) at 1:1000. Anti-FLAG polyclonal antibody was diluted in blocking buffer at 1:4000) Anti-FLAG was followed with horseradish peroxidase–conjugated anti-rabbit immunoglobulin G antibody at 1:4000 at room temperature for 30 minutes. Immunoreactive complexes on the membranes were visualized using enhanced chemiluminescence or enhanced chemiluminescence–plus detection reagent (GE Healthcare UK Ltd, Buckinghamshire, UK).

# RESULTS

## Genetic Analysis

We identified a novel heterozygous missense mutation c.1214G>A (p.R405K) in Exon 9 of *MYOT* in 1 LGMD patient (Fig. 1B). This mutation was not identified in a panel of 100 healthy Japanese controls.

## Clinical Data

The 57-year-old female patient presented with gait disturbance. She started experiencing difficulty in standing up and climbing the stairs by age 41 years. Her condition gradually progressed, and by age 50 years, she could not walk long distances and could not stand up or climb stairs without support. Her deceased father and elder sister had a similar condition. Her sister was previously diagnosed as having sporadic inclusion body myositis, but further information could not be obtained. On examination, the patient had proximal dominant muscle weakness, especially in neck flexors, iliopsoas, hamstring, and quadriceps muscles (3/5 by

manual muscle test), but no facial muscle weakness. She also showed a waddling gait and decreased deep tendon reflexes. Serum creatine kinase was mildly elevated (385 IU/L; normal, <200 IU/L).

## Histochemical and Immunohistochemical Analyses

Muscle tissue from the patient's vastus lateralis muscle showed marked variation in fiber size, scattered fibers with internally placed nuclei, and small angular fibers. There were scattered fibers with rimmed vacuoles (Fig. 2A). No obvious protein aggregates were seen. The intermyofibrillar networks were disorganized (Fig. 2B). Myosin ATPase staining showed an increase in the percentage of type 2C fibers (7%).

By immunohistochemistry, strongly immunoreactive aggregates of myotilin, αB-crystallin, ZASP, desmin (Figs. 2C–F), and actin (data not shown) were observed in a few fibers. Immunohistochemical and immunoblotting studies excluded other diagnosable causes of LGMD.

## Immunoblotting Analysis of Myotilin

The patient's muscle specimen showed an increased intensity of the 57-kd band corresponding to the amount of myotilin monomers compared with the band intensity in a control sample. On the other hand, the 110-kd band corresponding to myotilin dimer was fainter in the patient's sample than in the control muscle (Fig. 2G).

## Y2H Analysis for the MYOT Mutation

To determine the effect of the p.R405K mutation on protein-protein interactions, we used a Y2H system. We first tested the homodimerization capacity of wild and mutant myotilin. We generated *GAL4* DNA-binding domain or activation domain constructs containing wtMYOT or mMYOT and cotransformed them to yeast. All MYOT double transformants grew on low-stringency plates, indicating that no MYOT constructs were intrinsically lethal to the yeast cells. Only wtMYOT double transformant grew on medium- and high-stringency plates; the wtMYOT and mMYOT transformant and the mMYOT double transformant did not grow. These results indicate defective dimerization of mutant myotilin with both wild-type and mutant myotilin.

We next tested the interaction between myotilin and its known binding protein partners ACTA1, ACTN2, and FLNC. We cotransformed yeast with wtMYOT or mMYOT with each of ACTA1, ACTN2, and FLNC. The wtMYOT and ACTA1, mMYOT and ACTA1, wtMYOT and ACTN2, and wtMYOT

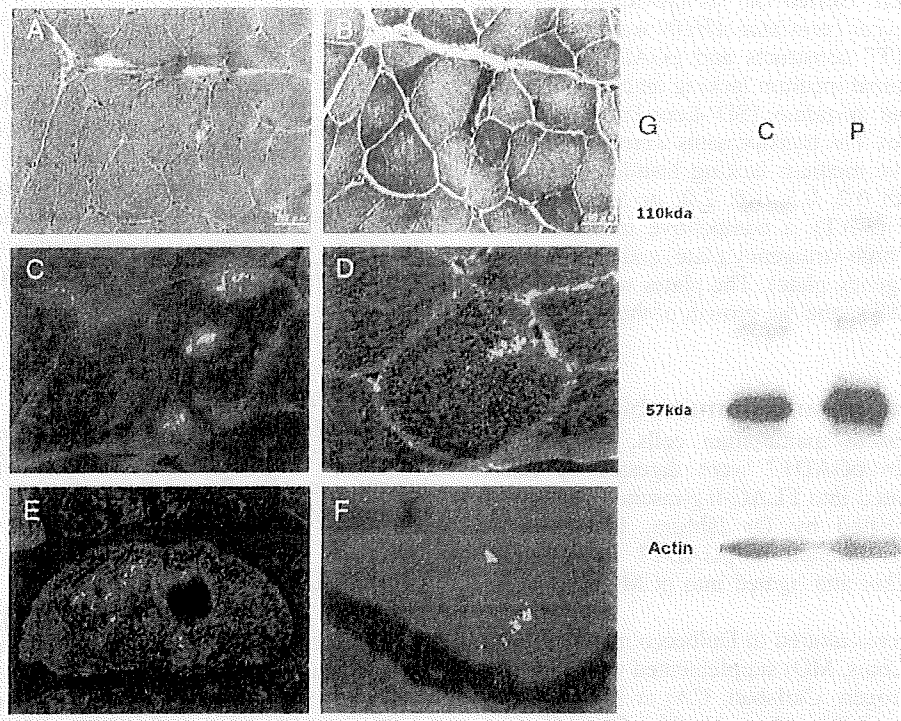


**FIGURE 2.** Histopathology and immunoblot of muscle from patient with p.R405K mutation. **(A)** Modified Gomori trichrome stain shows scattered fibers with rimmed vacuoles. **(B)** Nicotinamide adenine dinucleotide dehydrogenase–tetrazolium reductase stain shows myofibrillar disorganization. **(C–F)** Immunostaining reveals abnormal accumulation of myotilin **(C)**, desmin **(D)**, Z band alternatively spliced PDZ motif protein **(E)**, and αB-crystallin **(F)**. **(G)** Immunoblot analysis of myotilin in muscle from the patient shows an increased intensity of the 57-kd band that corresponds to monomeric myotilin and a decrease in intensity of the 110-kd band that corresponds to myotilin dimer compared with the control muscle sample. Scale bars = **(A, B)** 100 μm; **(C–F)** 20 μm. C, control; P, patient.